SCATTERING OF Co^{60} GAMMA RAYS AT 90°

A Dissertation

Presented to

the Faculty of Graduate Studies

at the University of Manitoba

In Candidacy for the Degree of

Master of Science

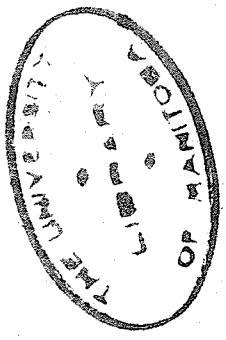

by

Jovan V. Jovanovic

1956

ABSTRACT

The elastic scattering of gammas of 1.17 MeV and 1.33 Mev from a Co^{60} source was measured for the scattering angle of 90^{o} and four different materials (Pb, Cu, Al and H_2O). Intensity of the source used was about 1000 curies and the scattered γ-ray spectrum was obtained by using a NaI(Tl) crystal ($1\frac{1}{2}$" thick and $1\frac{1}{4}$" diameter) and a single channel pulse height analyzer. The cross sections obtained are tabulated on page 59. These results agree fairly well with Bethe's form factor calculations for Rayleigh scattering and with the classical Thomson formula for elastic scattering by the nucleus.

The hard continuous gamma spectrum, usually ascribed to bremsstrahlung from photo- and Compton electrons, was examined for different thicknesses of Sn, Cu and Pb scatterers. The intensity of the spectra and the fact that it is almost independent of the scatterer thickness unambiguously proves that only a minor part of the hard component is caused by bremsstrahlung. The assumption that its origin is in the Compton effect on bound electrons seems consistent with the measurements.

Contents

List of figures

I INTRODUCTION

The scattering of a gamma ray by an atom can take place in several ways. The most probable process is Compton scattering from the atomic electrons, very well explained theoretically [1] and checked experimentally [2, 3] for the usual case where the electrons may be considered free and at rest. Here a gamma ray scattered at any angle has a definite energy given by the well-known Compton formula. The effect of electron binding is to give a distribution of energies to the scattered gamma rays as a result of the distribution of electron velocities within the atom [4]. This is well known in the X-ray region, but for higher energies the Compton line broadening has not been well treated theoretically or observed experimentally.

A process with much smaller probability is the elastic scattering which can occur in several different manners. In this case theoretical treatments have preceded experiments and four different elastic processes have been predicted. These are Rayleigh scattering by bound electrons [5, 6], Thomson scattering by the nucleus [7], Delbruck (potential) scattering from the electric field of the nucleus [8] and nuclear resonant scattering [9, 10]. All these four processes are coherent meaning that their scattering amplitudes must be added rather than their intensities. Since scintillation counter techniques have been developed, several successful experiments have been done on resonance scattering from

the nucleus as well as a number of experiments on Rayleigh and Thomson scattering [11-20]. Delbruck scattering has not yet been observed experimentally.

In all scattering experiments we must use scatterers of finite thickness. This has the effect that some secondary processes take place. Among these processes the annihilation of positrons created by gammas is the best known one [c.f. sec. 26, 27 in ref. 1, and for instance ref. 14]. Another secondary process is bremsstrahlung due to electrons produced by the photo- and Compton effects. The energy spectrum of the gammas created in this manner is evidently dependent on the scatterer thickness and covers continuously the range from zero to the maximum energy of the ejected photoelectrons. In almost all experiments on elastic scattering a hard* continuous component of gammas was observed [14, 15, 16, 19, 20] and has been ascribed to bremsstrahlung*.

The aim of this experiment was to get some more data on the elastic cross section for different atomic numbers (particularly for low Z) and to investigate more closely the origin of the hard continuous component. In section I a short theoretical discussion of scattering processes is presented in the scope that will be necessary for the discussion developed in section V. In section II and III the experimental set up and method are explained and the results obtained are presented in section IV.

---

* See, however, Mann [19] who suggests Compton effect on bound electrons for part of it.

* By hard we mean γ-rays of energies higher than the energy of gammas scattered by the Compton effect.

II. THEORETICAL CONSIDERATIONS.

(A) Main primary processes.

(a) Photo effect.

For the discussion that follows the experiment we need to know roughly the angular distribution of ejected photo-electrons. We are not particularly interested in the total cross section for photo effect, so we shall present only the angular dependence of the differential cross section. Also, because the experimental results show that about 80 per cent of the photo electric absorption occurs in the K-shell for γ-ray energies of .5 MeV or higher we shall not consider here effects in the L-shell.

Several formulas for the differential cross section have been derived all having a limited range of validity. Sauter [21] has derived one that is most applicable in our case. It is valid for relativistic energies of the ejected photoelectrons and for $Z \ll 137$. Its angular dependent part for the case of an unpolarized primary beam is

$$\sigma(\theta) \sim \sin^2\theta \left[\frac{\pi \sqrt{1-\beta^2}}{(1-\beta\cos\theta)^4} - \right.$$

$$\left. - \frac{\pi (1-\sqrt{1-\beta^2})}{2\sqrt{1-\beta^2}(1-\beta\cos\theta)^3} + \frac{(1-\sqrt{1-\beta^2})}{4(1-\beta^2)(1-\beta\cos\theta)^3} \right] \qquad (2.1)$$

where (θ) is the angle between the direction of the ejected electron and the direction of the primary photon, and β is the ratio of velocity of photoelectrons to the velocity of light.

It can be easily shown from the above formula that in the case when the energy of the ejected photoelectrons is 1.2 MeV (this is applicable to the radiation from Co^{60}) almost all of the electrons are emitted within an angle of 25° with the primary beam.

(b) Compton effect

From the relativistic relations for the energy and momentum it is easy to obtain the familiar equation that expresses the energy E of the scattered photon in terms of its primary energy E_0 and the scattering angle Θ i.e.

$$E = \frac{E_0}{1 + \gamma(1 - \cos\Theta)} \,. \qquad (2.2)$$

Here $\gamma = E_0/mc^2$, where mc^2 is the rest energy of the electron.

The differential cross section $\frac{d\sigma(\Theta)}{d\Omega}$ * for the process is given by the well-known Klein-Nishina formula (ref. [1] p. 219, eq. (40)). In the nonrelativistic case ($\gamma \ll 1$) it tends to a limit

$$\frac{d\sigma(\Theta)}{d\Omega} = r_0^2 \frac{1 + \cos^2\Theta}{2} \qquad (2.3)$$

where $r_0 = e^2/mc^2 = 2.82 \times 10^{-13}$ cm is the classical electron radius. This expression was initially derived by J.J. Thomson on purely classical grounds.

From the Klein-Nishina formula for the recoiling electrons (ref. [1], p. 220, eq. (43)) or from its graphs [22] it can be deduced that most of the recoil electrons go in

* $\frac{d\sigma(\Theta)}{d\Omega}$ is the cross section for scattering per unit solid angle.

the forward direction, and from eq. (2.2) it is clear that these electrons have the largest energies.

(c) Pair production

The differential cross section for the creation of a pair (ref [1], p. 257, eqs. (6) and (7)) shows that the angular distribution of positrons is strongly peaked in the forward direction and that the cross section for pair creation is proportional to Z^2. For heavy elements and relativistic energies and in the case of screening there is a small correction factor that slightly changes the Z^2-dependence.

(B) Secondary Processes

(a) Bremsstrahlung due to photo and Compton electrons.

The differential cross-section for bremsstrahlung has been derived theoretically by several authors (section 25 in ref. [1]) but recent experiments of Motz [23] have shown that the theory does not give satisfactory results. We reproduce in fig. (1), in a convenient and simplified form, his results for the cross section for 1 MeV electrons at 90°. Cross sections for Cu and Su have been interpolated using theoretically obtained Z^2-dependence that is valid for low Z. (ref. [1], sec. 25).

(b) Annihilation of positrons at rest and in flight.

When positrons are annihilated at rest two γ-quanta of energy 511 KeV are produced and their angular distribution is isotropic.

The probability for the annihilation of a positron when it collides with a negative electron is treated in ref. [1] (sec. 27, subsection 1) for the case when the centre of mass of both electrons is at rest. In order to get the differential cross section for the annihilation in flight it is necessary

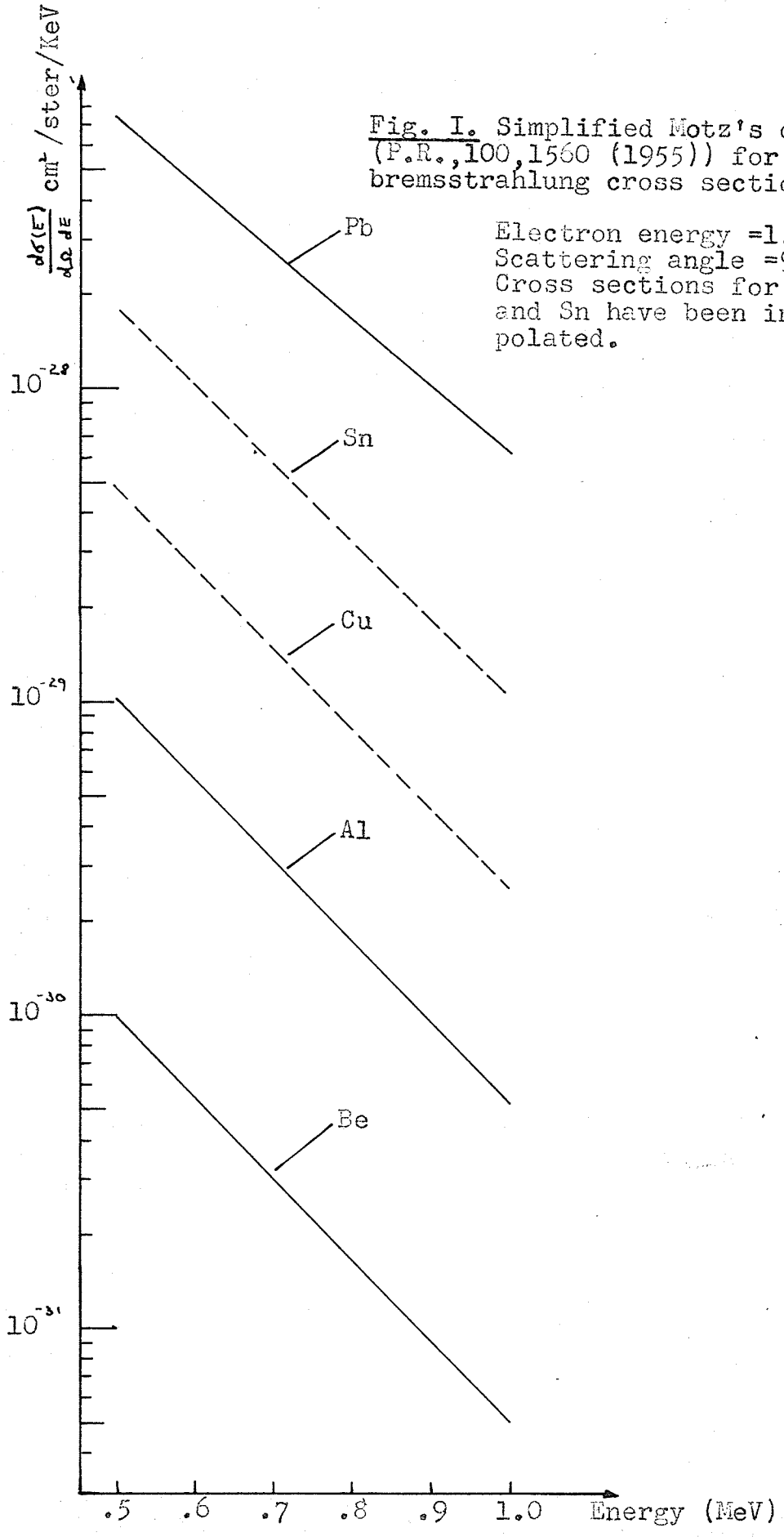

Fig. I. Simplified Motz's data (P.R., 100, 1560 (1955)) for the bremsstrahlung cross section.

Electron energy =1.0 MeV
Scattering angle =90°
Cross sections for Cu and Sn have been interpolated.

to make a simple Lorentz transformation [24]. Energies of γ-rays created $(h\nu)_1$ and $(h\nu)_2$ are directly related to the angle Θ one of them make with the original direction of positron. So, it can be shown (ref. [24] eq. 2) that

$$(h\nu)_1 = \frac{mc^2}{1 - \frac{E - mc^2}{E + mc^2} \cos\Theta} \tag{2.4}$$

and of course

$$(h\nu)_2 = E + mc^2 - (h\nu)_1 \tag{2.5}$$

Here, E is the total energy and mc^2 is the rest energy of a positron.

Besides this two quanta annihilation a positron can combine with an electron and produce three quanta, or only one. For small positron energies these processes are very improbable with respect to two quanta annihilation and usually their effects can be neglected [25].

(C) Less probable primary processes.

(a) Thomson scattering

The Compton effect on the nucleus exists as well as on electrons and the discussion reviewed in section (A-b) is applicable in this case, too. But because the mass M of any nucleus is much greater than the mass of the electron we have that

$$\gamma = \frac{E_0}{Mc^2} \ll 1$$

Consequences are that the scattering of photons is elastic (see eq. (2.2)) and that the scattering cross section is

given simply by the classical Thomson formula (2.3) where r_0 is replaced now by $(Ze^2)/Mc^2$. That is

$$\frac{d\sigma_T}{d\Omega} = \frac{(Ze)^4}{(Mc^2)^2} \frac{1+\cos^2\theta}{2} \tag{2.6}$$

or introducing the atomic weight A and substituting numerical values for the universal constants we have

$$\frac{d\sigma_T}{d\Omega} = 2.39 \times 10^{-32} \frac{Z^4}{A^2} \frac{1+\cos^2\theta}{2} \tag{2.7}$$

(b) Rayleigh scattering

Elastic scattering of γ-rays by bound electrons, usually called Rayleigh scattering, or electron resonance scattering, may be treated in the following way: a primary photon is absorbed by an atomic electron that is excited to an energy state in the discrete or continuous spectrum.

It has been shown that in the non-relativistic limit the amplitude for Rayleigh scattering a_R can be expressed as the ordinary Thomson scattering amplitude a_T corrected by an atomic form factor, i.e.

$$a_R = a_T \cdot F(q) = \frac{e^2}{mc^2}\sqrt{\frac{1}{2}(1+\cos^2\theta)}\cdot F(q) \qquad (2.8)$$

where q is the change of momentum of the photon that is

$$q = 2\frac{h\nu}{c}\sin\frac{\theta}{2} \qquad (2.9)$$

and, as shown by Franz [5], $F(q)$ is the form factor

$$F(q) = \int u\, e^{i\vec{q}\cdot\vec{r}}\, u\, d^3\vec{r}$$

where $\bar{u}u$ is the charge density. Franz used the following simplifying assumptions: (a) the Thomas-Fermi electronic charge distribution; (b) the assumption that the change of the momentum of the photon is much smaller than mc i.e. $q \ll mc$; (c) that the velocity v of the electron that scatters the quantum is non-relativistic, i.e. $(v/c)^2 \sim (\alpha Z^2/n)^2 \ll 1$ where α is the fine structure constant and n is the principal quantum number; and (d) he neglected binding in the intermediate state, i.e. he used plane wave functions. By this method he obtained the following result

for the scattering amplitude a_F

$$a_F = \frac{e^2}{mc^2}\sqrt{\tfrac{1}{2}(1+\cos^2\theta)}\,\frac{Z}{u}\sqrt{\frac{\pi}{2u}} \qquad (2.10)$$

where

$$u = 1.21\times 10^{-3}\,\frac{Z^{1/3}}{mc}\cdot q \qquad (2.10')$$

The corresponding cross section, providing that other forms of coherent scattering are negligible, is

$$\frac{d\sigma_F(\theta)}{d\Omega} = \frac{e^4 Z^2}{(mc^2)^2}\,\frac{u}{2u^3}\,\frac{1+\cos^2\theta}{2} \qquad (2.11)$$

or, by putting in numerical values

$$\frac{d\sigma_F(\theta)}{d\Omega} = \frac{8.67\times 10^{-33}}{u^3\,\frac{\theta}{2}}\left(\frac{Z\cdot mc^2}{h\nu}\right)^3\frac{1+\cos^2\theta}{2}\ \text{cm}^2/\text{steread} \qquad (2.11')$$

The scattering amplitude a_F is in phase with a_T due to Thomson scattering so that the differential cross section σ_{TF} in the case where neither of these two processes is negligible is

$$\frac{d\sigma_{TF}(\theta)}{d\Omega} = a_T^2 + a_F^2 + 2\,a_T a_F \qquad (2.12)$$

Theoretical calculations of the scattering amplitude for this process applicable to a general case have not yet been made. Bethe [26] has calculated the contribution (of K electrons only) to the scattering amplitude using Dirac wave functions, neglecting binding energy in the intermediate states and assuming that changes of the photon momentum are larger than the characteristic momentum of K electrons. i.e.

$$q \gg \frac{mc\,Z}{137}$$

He has shown that, in this case, the scattering amplitude a_B is still given by eq. (2.9) where the form factor is

$$F(q') = \frac{\sin(2\gamma \tan^{-1} q')}{\gamma q' (1+q'^2)^{\gamma}} \tag{2.13}$$

here

$$q' = \frac{137}{Z}\frac{h\nu}{mc^2}\sin\tfrac{1}{2}\theta \tag{2.13'}$$

and

$$\gamma = \sqrt{1-(Z/137)^2} \tag{2.13''}$$

This, Bethe's expression for the scattering amplitude a_B

$$a_B = \frac{e^2}{mc^2}\sqrt{\tfrac{1}{2}(1+\cos^2\theta)}\,\frac{\sin(2\gamma\tan^{-1}q')}{\gamma q'(1+q'^2)^{\gamma}} \tag{2.14}$$

is again in phase with the scattering amplitude a_T due to Thomson scattering so that the differential cross section, provided that the contribution due to other elastic processes is negligible, is

$$\frac{d\sigma_{TB}(\theta)}{d\Omega} = a_T^2 + a_B^2 + 2a_T a_B \tag{2.15}$$

Rohrlich and Rosenzweig [27] have extended Bethe's calculation to the case of L-electrons. They have shown (p. 388 in [8]) that at intermediate energies (momentum transfer $\sim \alpha Z m$) the contribution of the L-electrons to the differential cross section for the elastic scattering is about 20% of that due to K-electrons. With this modification the eq. (2.15) becomes

$$\frac{d\sigma_{TB}(\theta)}{d\Omega} = a_T^2 + 1.44\,a_B^2 + 2.4\,a_T a_B \tag{2.16}$$

Levinger [6] has calculated some corrections to Bethe's form factor formula mainly applicable to small angles. We shall not discuss them here because our scattering angle is 90°.

Brown et al. [28] have shown that taking into account the binding energies of the intermediate states may change the expression for the scattering amplitude significantly. Unfortunately these calculations are also inapplicable to the elastic scattering of Co^{60} γ-rays at 90° although they are now being extended.

(c) Delbrück scattering

The interaction of strong electric fields with a photon may cause a change in its momentum. Because only atomic nuclei can produce fields strong enough and the mass of the nucleus is large, the energy of nuclear recoil is negligible and the scattering is elastic. This scattering is frequently refered to as potential scattering of light. The process takes place through an intermediate state. Two intermediate states are possible, one where an electron pair is actually produced and immediately again annihilated, and the second where the pair is only virtually produced.

Theoretically, the problem is very complicated. It has been possible to carry out calculations analytically only for the scattering angle of 0°, and this has been done by Rohrlich and Gluckstern [29] and Toll [30]. Some approximate

calculations have been done also for very small scattering angles and for very high energies [31].

Evidently no calculations can be applied to our experiment and in the discussion of the results the contribution due to potential scattering cannot be taken into account.

(d) Resonance scattering from the nucleus.

There are two different cases of resonance scattering, one when the photon energy is near resonance and the other when it is far from resonance. The cross section, when the photon is near resonance is high, of the order of a barn or still higher but the resonance is very narrow (always narrower than 10^{-2} eV). So the photon is usually off the resonance except in very special circumstances. In spite of that fact, several successful measurements on resonance scattering have been done [9, 10].

The second case is when the photon energy is far from the resonance. The effect of the tail of the "giant resonance" could be appreciable. This effect has been treated theoretically by Levinger [32] for the case of $Z > 50$ because measurements on photonuclear reactions indicate the existence of this "giant resonance" at excitation energies of 15-20 Mev. He has shown that in a hypothetical case when only Thomson and resonance scattering are present the differential cross section is

$$\sigma^2 = (a_{NR} + a_T)^2 \cong a_T^2 \left[1 - 2\left(\frac{h\nu}{E_a}\right)^2 \left(\frac{N}{Z}\right)(1 + .8\alpha) \right] \qquad (2.17)$$

where a_{NR} is the scattering amplitude due to nuclear resonance scattering, E_a is the nuclear excitation energy (~15 Mev), N is the number of neutrons in the nucleus and α (= $\frac{1}{2}$) is the fraction of exchange force. From this formula, it can be easily shown that in the case of lead and γ-rays from Co^{60}, the contribution due to resonance scattering is smaller than 1% of that due to Thomson scattering.

The case of light elements has not yet been treated theoretically but it is expected that the contribution is again small.

(e) Compton scattering on bound electrons

The collision of a photon with a free electron at rest (Compton effect) changes its initial energy by an amount determined by eq. (2.2). The energy change is quite different if the electron has an initial momentum $\vec{p}$ and is a function of $\vec{p}$ as well as θ. For instance, by using the conservation laws for energy and momentum it can be easily shown that, for the angle $\theta = 90°$, a scattered photon can have, for different values of $\vec{p}$ any energy from zero to twice the initial energy. If the photon is scattered backward or forward there is no limit to its energy at all, (as the electron momentum approaches ∞).

According to the Bohr picture of the atom every bound electron has a definite momentum that is dependent on the principal quantum number. According to wave mechanics there exists for every bound electron a continuous linear momentum distribution. It is clear that, at least energetically, the Compton

effect on bound electrons must produce a broad continuous energy spectrum of scattered photons peaked about the energy given by eq. (2.2).

In the X-ray region the Compton effect on bound electrons has been investigated thoroughly (p. 238-255 in ref. [2], [4] and [33]) for the case when the scattered photon has an energy close to that given by eq. (2.2). It was shown by Wentzel (p. 243 in ref. [2]) that the broadening of the modified (Compton) line due to scattering by an electron bound in a particular level is dependent on the binding energy of that level (E_b). The energy width (ΔE) of the modified line is approximately

$$\frac{\Delta E}{E_o - E_c} \sim \sqrt{\frac{E_b}{E_f}} \sim \sqrt{\frac{E_b}{E_o - E_c}} \qquad (2.18)$$

or

$$\Delta E \sim \sqrt{E_b (E_o - E_c)} \qquad (2.19)$$

Here, E_o and E_c are the energies of primary beam and Compton line respectively, and E_f is the kinetic energy of the recoiling electron.

Duncanson and Coulson [33] have calculated the Compton profiles (shape of the modified line) for a few light atoms by using the distribution of electron momenta in the atom as obtained from electron wave functions. They have shown that the contribution to the Compton profile of electrons is in first approximation additive and in the case of 1s-electrons

the Compton profile $J_{1s}(q)$ is equal

$$J_{1s}(q) = \frac{8\alpha^5}{3\pi(q^2+\alpha^2)^3} \qquad (2.20)$$

Here, $\alpha = \frac{Z}{a_0}$ ($a_0 = \frac{\hbar^2}{mc^2}$ is the Bohr radius) and q is a convenient variable which depends on the energy of the primary gammas, the angle of scattering and the difference between the energy of a scattered photon and E_c. It is equal to zero for the case when the scattered energy is equal to E_c.

The above formula are valid only in the non-relativistic case but it is expected that they are correct within an order of magnitude in the relativistic case, too.

III. EXPERIMENTAL ARRANGEMENT

The experiment was performed by using the A.E.C.L. Cobalt-60 Beam Therapy unit No. A-5 installed in the Winnipeg General Hospital whose source strength was about 1000 curies. Scattered γ-rays were analyzed by a standard scintillation spectrometer.

(a) Geometrical set up

The geometrical arrangement of the source, scatterer, lead shields and NaI crystal is shown in Fig. (2). The drawing is 1/8 full scale. The source is labelled by S, scatterer by St, NaI crystal by C and photomultiplier by P. The primary and secondary diaphragms(they are part of the unit) and lead shield around the crystal are marked by PD, SD and LS, respectively. Very strong radiation scattered by the Compton effect was filtered by a lead filter (F). Uniformity of the beam was not checked. Position of the scatterer was fixed by the help of the cross hairs (CH) at the mouth of the beam unit and of a light source (not shown on the drawing) installed in the unit.

The average scattering angle was 90°. Scatterers of different sizes and thicknesses were used. The largest scatterer used ($5\frac{1}{2}$" x 6") subtended an angle of about 35° at the crystal and the smallest one (1 " x $1\frac{1}{2}$") about 17° . Distance from the center of the source to the center of the scatterer was 92.5 ± .5 cm.

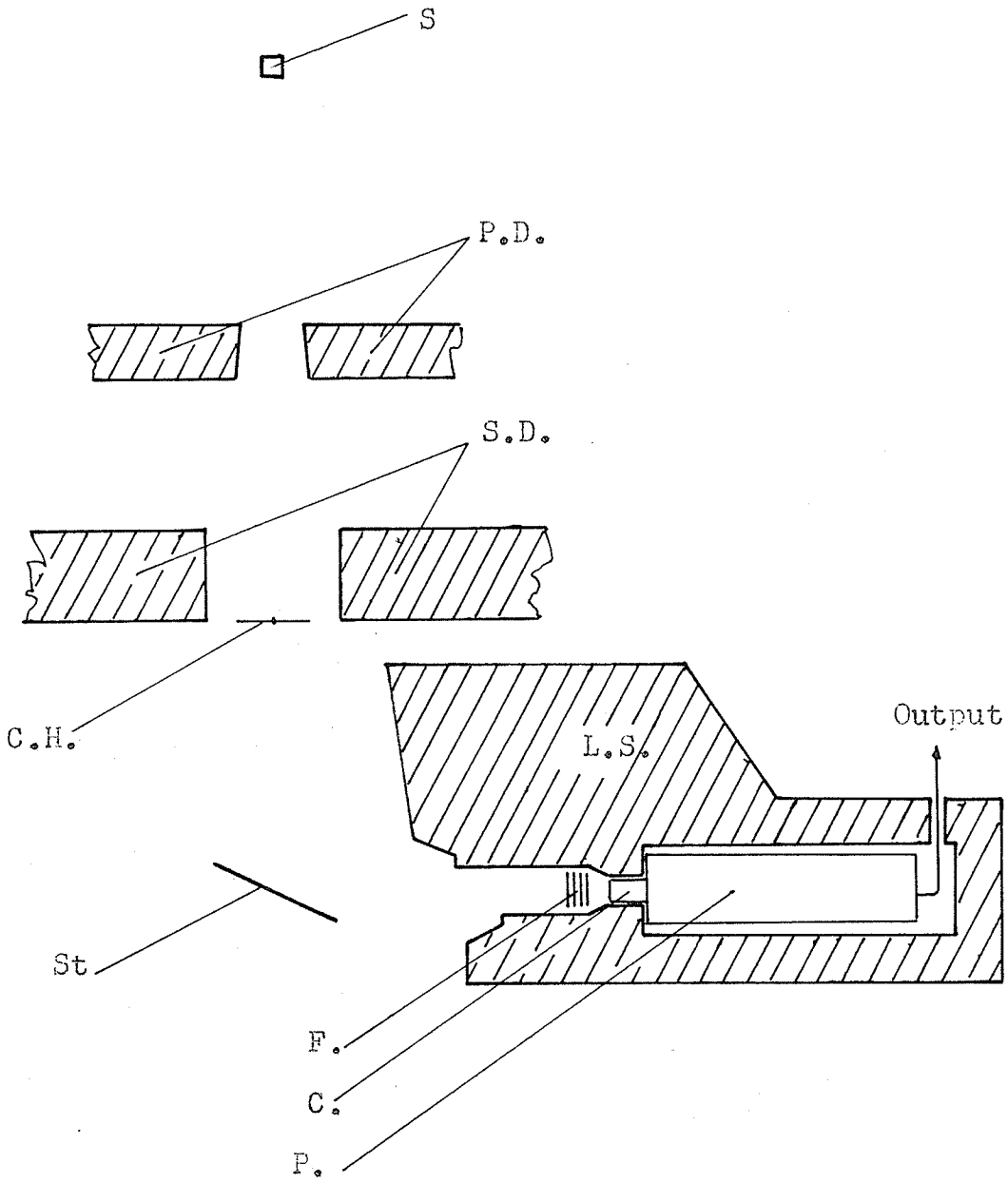

Fig.2. Sketch of the geometrical arrangement of the source, scatterer and crystal.

The drawing is 1/8 full scale. For the explanation of letters see sec. III-a.

(b) Scintillation spectrometer

The scintillation spectrometer was of a conventional type. A NaI crystal (size $1\frac{1}{4}$" in diameter and $1\frac{1}{2}$" long) was mounted on a 6292 DuMont photomultiplier tube followed by a cathode follower, amplifier, single channel pulse height analyzer and scaler. An oscilloscope was used for visual check of the equipment. Drifts of the spectrometer were usually smaller than 3% over the measuring periods of 10 hours—due to this relatively large drift the equipment was usually calibrated every three quarters of an hour by a small Co^{60} source (about 0.1 mC). Two different channel widths were used, 2.8Volts and 0.75 Volts but the stability of the channel width was not checked directly. Energy calibration of the spectrometer was done by using the 1.33 MeV and 1.17 MeV lines from Co^{60} whose disintegration scheme is given in Fig. (4) [34], the 1.12 MeV line from Zn^{65}, the 660 KeV line from Cs^{137} and the .511 MeV and 1.28 MeV radiation from Na^{22}. The calibration curve is shown in Fig. 3. Resolution of the spectrometer was 11.5% for the 660 KeV line from Cs^{137} with a channel width of 2.8 Volts and 8% for 1.1 MeV line from Zn^{65} with a 0.75 Volt channel.

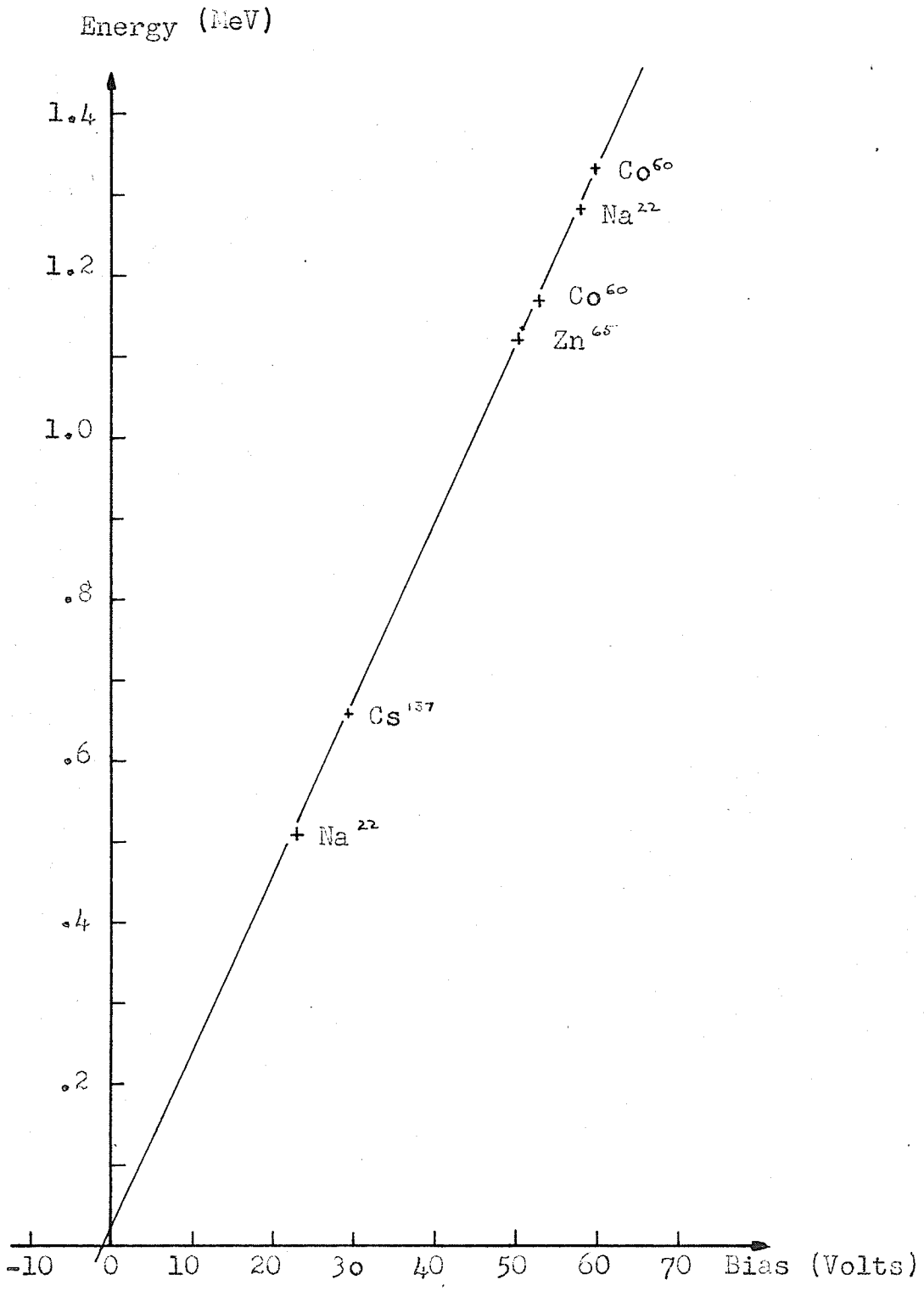

Fig.3. Energy calibration curve for the scintillation spectrometer.

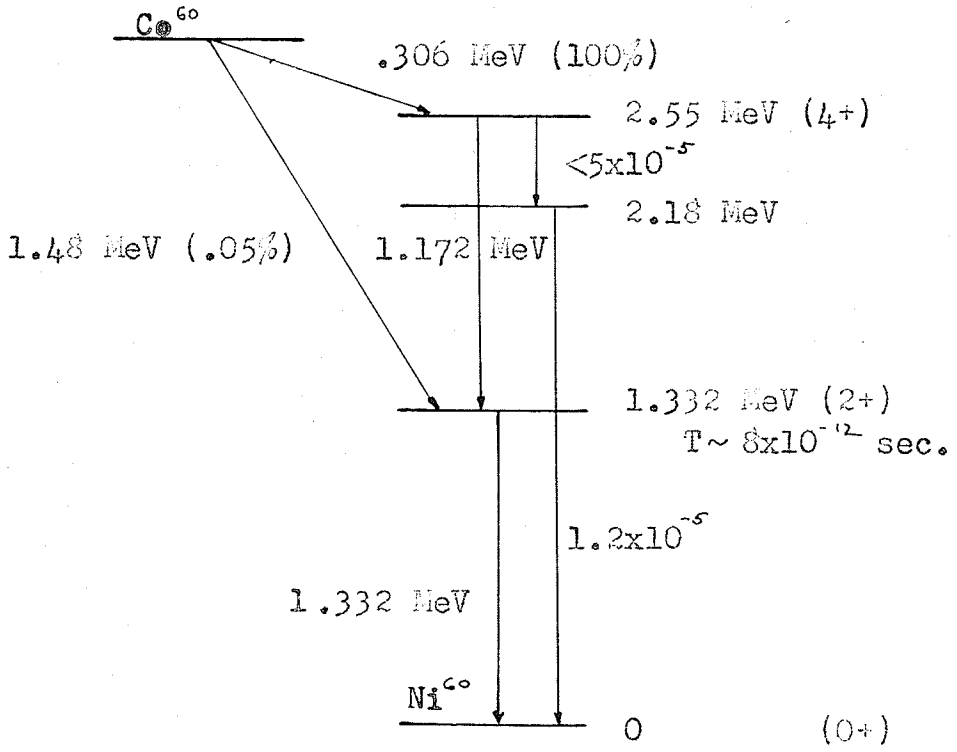

Fig.4. Disintegration scheme of Co^{60}.

IV METHOD

In this section we shall present formulas used in evaluating and estimating cross sections for elastic and inelastic scattering. Measurements and results which are common to all scatterers used will be discussed here, too.

(a) Elastic scattering

We make the following simplifications:

(1) We consider a parallel beam of monochromatic primary radiation whose energy is E_0.

(2) We assume a solid angle (scatterer-crystal) small enough so that we may neglect the change of the differential cross section in this angular interval.

(3) We assume that the length of the scatterer is much greater than its thickness so that we may neglect the effect of the edges of the scatterer on the correction due to absorption in it.

(4) We neglect, for the time being, the correction due to finite size of the scatterer, i.e. the fact that one side of it is nearer to the crystal than the other, and that the crystal efficiency for different parts of the scatterer is different.

With the help of Fig. 5 it may be easily deduced that the number of photons scattered by the scatterer per steradian at an angle Θ is

$$\int K' S \frac{d\sigma(\theta)}{d\Omega} \int_0^t e^{-\tau_0(\rho x)\Psi} \, dx \tag{4.1}$$

(4.2)

where

$$\Psi = \left(\frac{1}{\sin \tau} + \frac{1}{\sin(\theta - \tau)} \right) \tag{4.2}$$

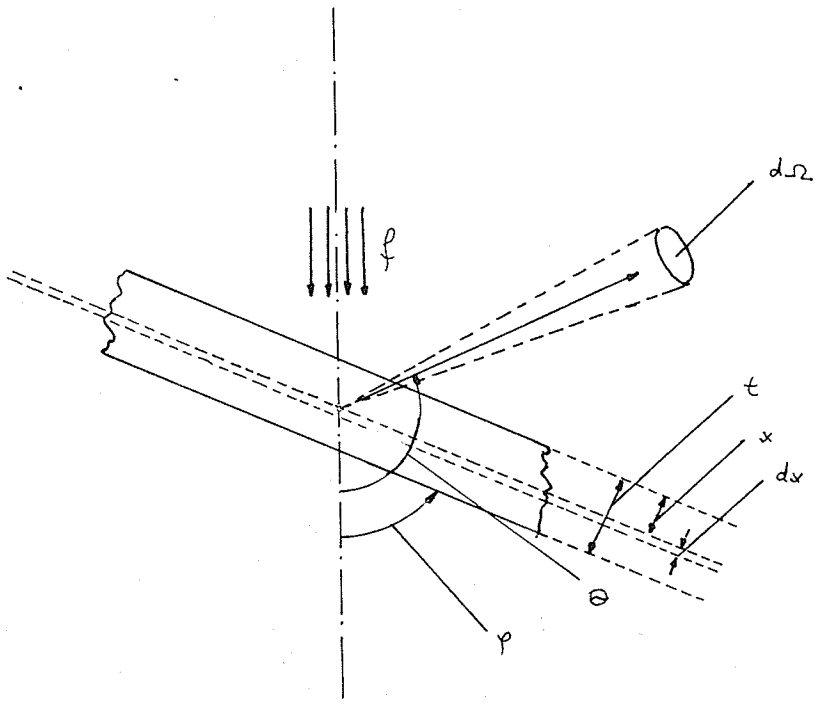

Fig. 5. Absorber position with respect to the primary and scattered beam.

and meanings of θ, φ and x are clear from Fig. 5.

The following notation was used.

ϕ = primary flux of photons in no. of photons traversing 1 cm^2 per second.

K' = no. of scattering atoms/cm^3

S = area of the scatterer in cm^2 .

t = thickness of the scatterer in cm.

$\frac{d\sigma(\theta)}{d\Omega}$ = differential cross section in cm^2/steradian.

τ_0 = mass absorption coefficient in cm^2/gm.

ρ = density of material in gm/cm^3 .

After the integration is performed we have that the no. of photons scattered per steradian is

$$\phi K \frac{d\sigma(\theta)}{d\Omega} \frac{1}{a} \tag{4.3}$$

where

$K = K'St$ = total number of atoms in the scatterer

$$\frac{1}{a} = \frac{1 - \exp[-\tau_0(t\rho)\Psi]}{\tau_0(t\rho)\Psi} \tag{4.4}$$

The number of pulses, N that is registered by the spectrometer when the position of the channel is set in the middle of the photo-peak is proportional to this number, i.e.

$$N = k \frac{\phi K}{a} \frac{d\sigma(\theta)}{d\Omega} \tag{4.5}$$

k is a constant that includes the solid angle subtended by the counter, a factor due to absorption in the lead filter, efficiency of the crystal and the effect of the finite channel

width of the spectrometer. k is usually unknown, but we can eliminate it by using an auxiliary small source of Co^{60} that has the same shape as the scatterer and which is placed in its position. The number of pulses N_s registered by the spectrometer under the same conditions as before is

$$N_s = k s_o \tag{4.6}$$

where intensity of the auxiliary source is $4\pi s_o$ disintegration/sec. By the help of eq. (4.6) we can eliminate k from eq. (4.5) and we get

$$N = N_s \frac{f}{s_o} \frac{K}{a} \frac{d\sigma(\theta)}{d\Omega} \tag{4.7}$$

If the intensity of the primary source which is used in the measurements is $4\pi S_o$ dis/sec/ and if r is the distance source-scatterer in cm, than

$$f = \frac{S_o}{r^2} \tag{4.8}$$

and after substituting in eq. (4.7) we have

$$N = N_s \frac{S_o}{s_o} \frac{K}{r^2} \frac{1}{a} \frac{d\sigma(\theta)}{d\Omega} \tag{4.9}$$

From this equation we see that we need not know the absolute strength of either source, S_o and s_o, but only their relative intensities.

Practically, the source s_o used has dimensions much smaller than the scatterer. Owing to this reason it is necessary to introduce another correction factor (b) that accounts for the finite size of the scatterer. By introducing it in the eq.(4.9) we have

$$N = N_s \frac{S_o}{s_o} \frac{K}{r^2} \frac{b}{a} \frac{d\sigma(\theta)}{d\Omega} \tag{4.10}$$

or

$$\frac{d\sigma(\theta)}{d\Omega} = \frac{N}{K}\frac{s_o}{S_o}\frac{r^2}{N_s}\frac{a}{t} \qquad (4.11)$$

(b) Continuous inelastic distribution of gammas.

In the introduction and in section II the existence of a continuous inelastic distribution was discussed. In this section we develop an approximate formula enabling us to evaluate the cross section for this type of scattering when the pulse height spectrum is measured. For such a process the differential cross section must be dependent on the energy (E) of the scattered gammas as well as on the angle (Θ). In other words $\sigma(E,\theta;E_o)dE$ expresses the probability that a scattered photon will have direction in a unit solid angle situated around Θ and energy in the interval E, $E+dE$, when the primary photon energy is E_o. Owing to this continuous energy distribution of scattered photons and to the fact that each monochromatic beam of gammas gives another continuous spectrum of pulses in the spectrometer it is clear that the pulse distribution as seen by a single channel analyzer is very complicated.

Because the statistical and other errors of the experimental results are large we use a very approximate formula to give us some information on cross sections. It can be expected that the results are good only to an order of magnitude. In developing this formula the following approximations were introduced, in addition to the four already used:

(5) We assume that the width at half height of the photo peak is small compared to the channel width.

(6) We consider the primary beam from Co^{60} as monoenergetic with an average energy of 1.25 MeV.

It can be easily seen with these six approximations that the number of pulses counted in a channel whose width in energy units is ΔE is equal to

$$N(E) = k(E) \int K \frac{d\sigma(E,\theta)}{d\Omega} \frac{\Delta E}{a(E)} \qquad (4.12)$$

Here the same notation as before is used except that the dependence on the energy E is explicitly shown.

If we have a source of gammas (energy E) whose strength is $4\pi s_0'$, than the number of counts due to it (under the same conditions as supposed in scattering of eq. (4.6)) is

$$N_s'(E) = k(E)\, s_0' \qquad (4.13)$$

We get in complete analogy with eq. (4.11) the cross section for the inelastic gamma distribution

$$\frac{d\sigma(E,\theta)}{d\Omega} = \frac{N(E)}{K} \frac{1}{N_s'(E)} \frac{s_0'(E)}{S_0} \frac{r^2}{b(E)} \frac{a(E)}{\Delta E} \qquad (4.14)$$

(c) Measurement of the relative strength of the sources S_0 and s_0.

Owing the great difference in the intensity of the sources S_0 (~1000 curies) and s_0 (~ 0.1 millicuries) this measurement was performed by using a source of intermediate strength s_m (~ 1 millicurie). The ratio of intensities s_0/s_m and s_m/S_0 was measured in two separate experiments.

The ratio s_0/s_m was measured directly, by placing the sources successively in the same position with respect to

the crystal and measuring the spectrum of its photo peaks corresponding to the 1.33 MeV line. By comparing the heights of the peaks, the following result was obtained.

$$\frac{S_o}{S_m} = 4.1 \pm 0.1 \qquad (4.15)$$

where the indicated error is the standard deviation.

On account of the tremendous strength of the source S_o it was not possible to measure S_m/S_o directly by a similar experiment. The following procedure was used: Source S_m was placed at the cross hairs (CH in Fig. 1) and the beam from S_o was shut off by the use of a mercury switch, already built in the beam unit. A copper scatterer, whose dimensions were 3" x 3" x .046", was placed at the standard position (St—Fig.1). On account of the small strength of S_m no lead filter (F - Fig.1) was used and the spectrum of the photo-peak due to gammas scattered by the Compton effect was taken. The height of this peak was taken and corrected for the presence of background whose spectrum was also measured. After that, the source S_m was removed, the scatterer was replaced by a thinner one (3" x 3" x .008") and the beam from S_o turned on. Intensity of the radiation scattered by the Compton effect was measured again. In this case, lead filters of five different thickness (from 5/8" to 9/8") were used, and after the counting rate was corrected for the presence of background it was extrapolated to zero thickness. This extrapolation was justified by the fact that the absorption

coefficient as obtained from this measurement agreed within 2% with that one from the tables (appendix I in ref. [9]).

By comparing the counting rates in the middle of the peaks and correcting for different distances source-scatterer in two cases the following result was obtained

$$\frac{S_o}{s_m} = 7.5 \times 10^5 \qquad (4.16)$$

Combining results (4.16) and (4.16) we have as the result

$$\frac{s_o}{S_o} = \frac{s_o}{s_m}\frac{s_m}{S_o} = 3.3 \times 10^{-7} \qquad (4.17)$$

the total possible error is fairly large; it is estimated it amounts about 20%.

(d) Correction for the finite size of the scatterer.

The correction factor ϵ (eq. 4.11) was measured by placing an almost point source s_o in twelve different positions corresponding to a scatterer whose size was $5\frac{1}{2}$" x 6" and whose angle φ (c.f. Fig. 2) was equal to 65° . By taking successively the counting rates at the top of the photo peak of the 1.33 MeV line the average of these twelve measurements was obtained. Comparing it with the counting rate due to the above source at the center of the scatterer it was found that, in the case of the above mentioned position and size of the scatterer, the correction factor was

$$\epsilon = 0.96 \pm 0.03 \qquad (4.18)$$

The indicated error is again the estimated total possible error. For other sizes and positions of the scatterers and

energies less than E_o = 1.33 MeV ℓ was not measured. In these cases, ℓ = 0.95 has been taken as a rough approximation.

(e) The measurement of N_s (eq. - 4.6)

N_s for the 1.33 MeV and 1.17 MeV lines was measured by placing the smallest Co^{60} source at the center of the scatterer and by using several different thicknesses of lead filter. In Fig. 6 the Co^{60} spectrum for this case is presented when the radiation was filtered through 7/8" of lead and the channel width was 2.8 Volts. Dotted and broken line correspond to the pulse height spectra due to monoenergetic gamma rays having energies 1.33 MeV and 1.17 MeV, respectively. They were obtained by decomposition of the Co^{60} spectrum (heavy line) by the help of measured pulse height spectra for Zn^{65} (1.12 MeV) and Na^{22} (1.28 MeV--shown on the same figure). In Fig. 7 are shown the absorption curves that correspond to similar measurements but with different thicknesses of lead filter. The absorption coefficients as deduced from these curves agree within 3% with the ones obtained from tables (appendix I in ref [9]).

Results for N_s (number of counts due to the auxilliary Co^{60} source) can be summarized in the following tables. Stated errors are estimated total errors.

Table I

Lead filter	(1.17 MeV)	(1.33 MeV)
0"	$(14.5 \pm 1.2) \times 10^3$	$(11.0 \pm .6) \times 10^3$
5/8"	$(5.3 \pm .8) \times 10^3$	$(4.20 \pm .13) \times 10^3$
7/8"	$(3.5 \pm .3) \times 10^3$	$(2.85 \pm .10) \times 10^3$
9/8"	$(2.3 \pm .2) \times 10^3$	$(1.90 \pm .08) \times 10^3$
14/8"	$(.84 \pm .07) \times 10^3$	$(.72 \pm .04) \times 10^3$

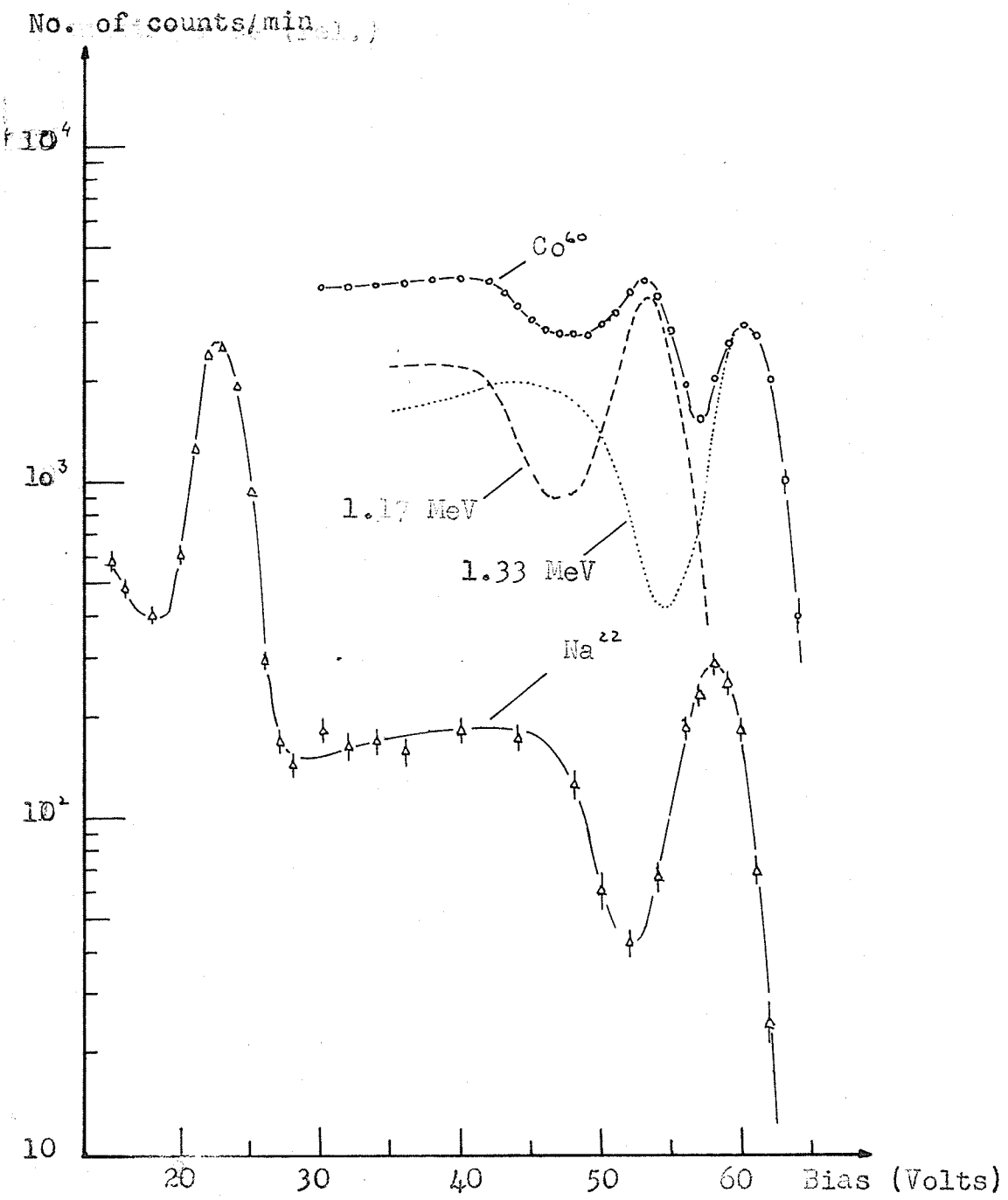

Fig.6. Pulseheight spectrum of Co^{60} and Na^{22}.

Circles (o) represent the Co^{60} spectrum when the radiation was filtered through 7/8" of lead. Dotted and broken lines are due to the decomposition of the Co^{60} spectrum into constituents.
Triangles (Δ) represent the Na spectrum taken without any filter.
Bars stand for the standard deviations.

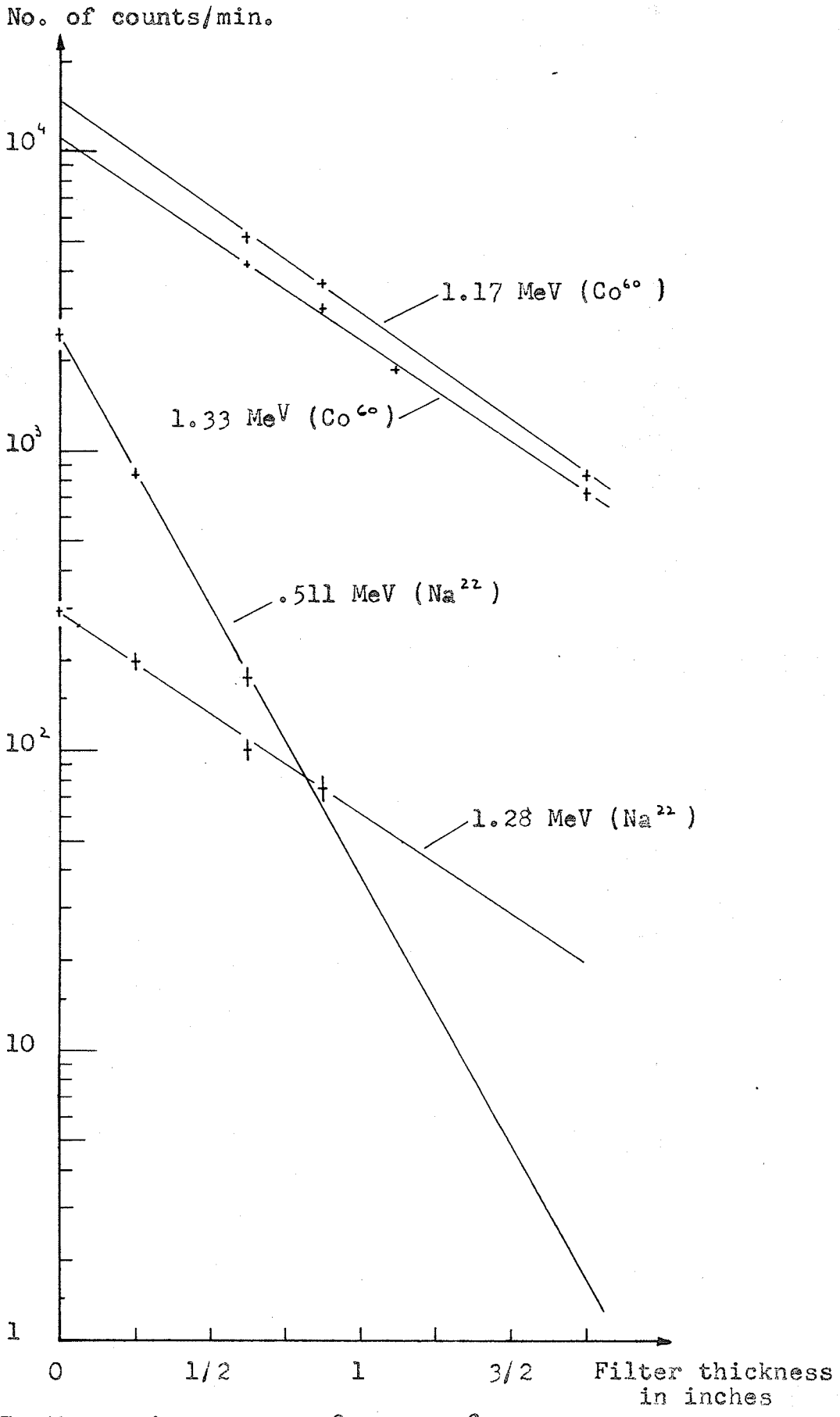

Fig. 7. Absorption curves of gammas from Co^{60} and Na^{22}.

In order to get a qualitative idea how $k(E)$ (from eq. 4.12) varies with energy, a similar measurement with Na^{22} was made. The result is also presented in Fig. 6 for the case when no lead filter was used. The measurements of the heights of both peaks was done for several different thicknesses of lead filter. The corresponding absorption curves are presented in Fig. 7; the absorption coefficients as calculated from these data are in fairly good agreement (within 3% error) with the coefficients from the tables (appendix I in ref. [9]).

This ratio of the intensities of the Na^{22} (δ_{Na}) and Co^{60} (δ_o) sources used was obtained by the following procedure. In Fig. 8, the no. of counts N_s for 1.33 MeV and 1.17 MeV line from Co^{60} (taken from Table I) for no lead filter were plotted. Then the number of counts due to the Na^{22} 1.28 MeV line was fitted assuming that the variation of N_s in the interval between the energies of the two Co^{60} lines was linear. The ratio of the no. of counts estimated in this manner to the actually observed number is taken as the ratio of the intensity of the two sources. i.e.

$$\frac{\delta_o}{\delta_{Na}} = 42.4 \pm 3.2$$

By using it, the number of counts due to .511 MeV line was recalculated (keeping in mind that 511 KeV line is twice as abundant as 1.28 MeV line) and plotted.

Heavy line (Fig. 8) represents interpolated dependence

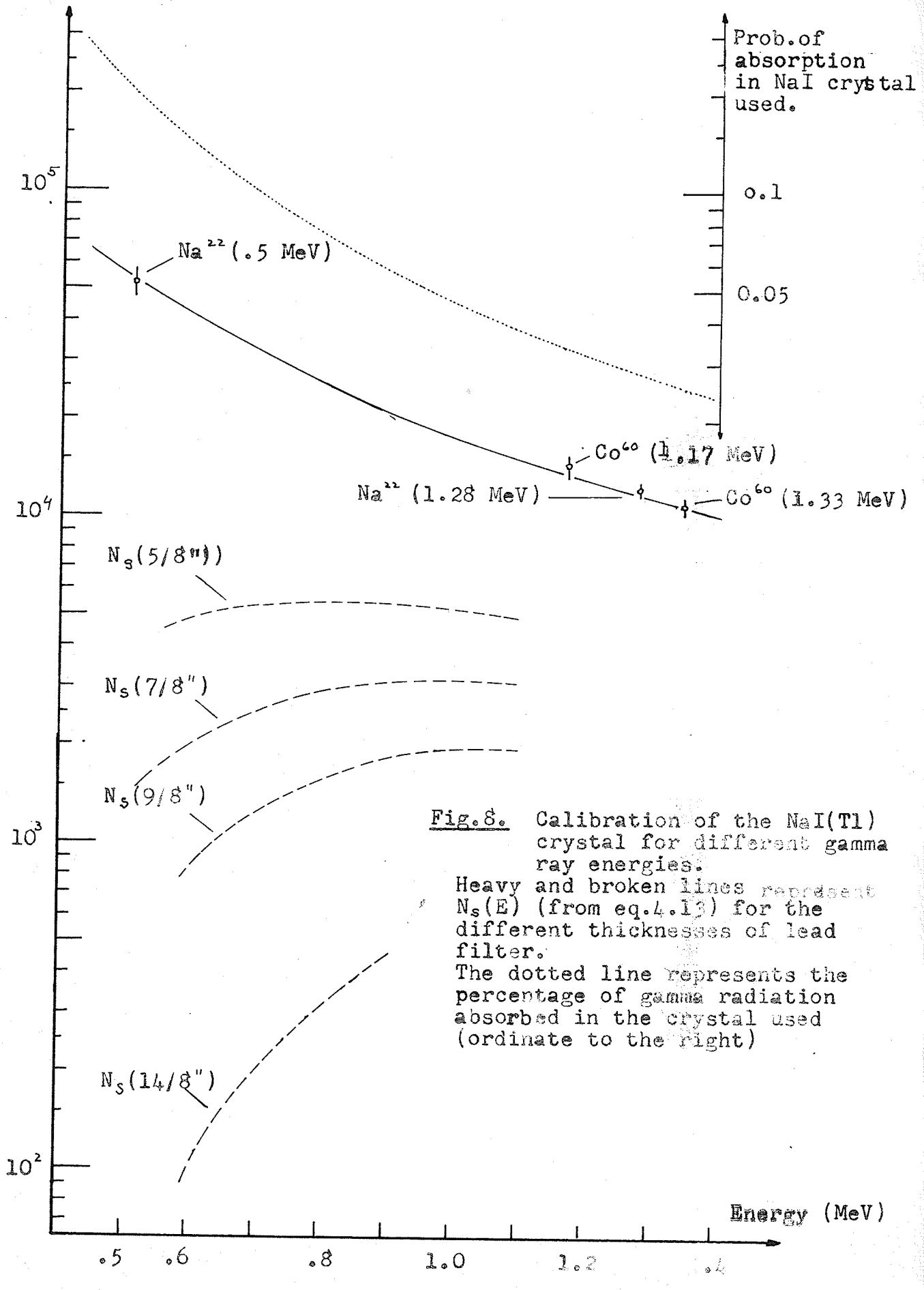

Fig.8. Calibration of the NaI(Tl) crystal for different gamma ray energies.
Heavy and broken lines represent $N_s(E)$ (from eq.4.13) for the different thicknesses of lead filter.
The dotted line represents the percentage of gamma radiation absorbed in the crystal used (ordinate to the right)

of N_s on energy E of gammas. Because the interval between 511 KeV and 1.17 MeV is fairly large the shape of the interpolation curve is estimated by the help of the dotted line. It was evaluated on the basis of data for the photo-absorption in NaI (p. 153, Fig. 17 in ref. [9]), and it represents the percentage of radiation absorbed in the crystal used assuming that the direction of gammas was along its axis. Broken lines at the bottom are obtained by correcting heavy line for the absorption in lead filter of different thicknesses (they are indicated in the figures) these curves are later mainly used in eq. (4.14) for evaluating the differential cross section $\sigma(\varepsilon,\theta)$.

(f) Measurement of the resolving time (τ).

A lead filter had to be used on account of strong intensity of the low energy gammas scattered by Compton effect. If it were not thick enough the pile up of pulses (when one pulse follows a preceding one in a time that is shorter than the length of the first pulse or to be more precise, shorter than the resolving time of the spectrometer) can significantly change the shape of the spectrum. In order to determine the thickness of lead that is just enough to make the number of pileup pulses negligible we need to know the resolving time τ (The number of pileup pulses is equal τN^2 where N is the counting rate). It was obtained by measuring the low energy spectrum of radiation scattered from two different water scatterers so adjusted that the number of pile up pulses in one case is quite appreciable and in another small.

The value obtained

$$\tau = (1.8 \pm 0.6) \times 10^{-6} \text{ sec} \qquad (4.20)$$

agrees qualitatively with the resolving time deduced from the shape of pulses as seen on the oscilloscope.

V. MEASUREMENTS AND RESULTS

In Figs. 9, 10, 11 and 14 are shown the measured pulse-height spectra at 90° for thick targets of H_2O, Al, Cu and Pb, respectively. It can be easily seen that they all have some common characteristics, ie. high intensity for pulse heights smaller than 25V (corresponding to energies of scattered gammas smaller than 600 KeV) and three or four peaks (in the case of H_2O and Pb there are only three) superposed on a continuous spectrum. Energies of gammas corresponding to this peak, as can be seen from the calibration curve in Fig. 3, are near 360 KeV, 511 KeV, 1.17 MeV and 1.33 MeV. These peaks are consistent with gammas scattered by Compton effect (360 KeV is the mean Compton energy corresponding to the two different lines in Co^{60} spectrum) annihilation radiation (511 KeV) and elastic scattering of the primary beam from Co^{60} (1.17 and 1.33 Mev). In the case of Pb there is only one unsymmetrical peak in the low energy range. The Compton peak and the annihilation peak are not resolved because the first is fairly broad due to very large size of the H_2O scatterer. Also, the large thickness of lead filter used (larger than in any other case) produced strong unsymmetrical absorption of a Compton peak favouring the higher energy radiation. In the case of Pb (Fig. 14) there is only a bump corresponding to 1.17 MeV . From the general shape of the spectrum it is clear that its presence is due to elastic scattering of 1.17 MeV photons that is masked by a

continuous pulse height distribution having a very steep slope in this region.

In Fig. 6 the Co^{60} pulse height spectrum filtered through 7/8" of lead is shown for the case when the source was placed in the center of the scatterer. Similar curves were obtained for all the other thicknesses of lead filter used. In order to separate the elastic pulse height spectrum from the measured one the above mentioned curves were used in the following way: the corresponding (with respect to the thickness of lead filter used) spectrum of the Co^{60} source was taken and so normalized that its 1.33 MeV peak made as good a fit as possible to the measured points. The top of the (normalized) Co^{60} peak was taken as N in eq. (4.11). This procedure was applied directly to the H_2O, Al and Cu scatterers because the continuous distribution had a small intensity in this region. The case of 1.17 MeV line will be discussed later as well as the Pb scatterer.

In order to get more insight into the origin of the continuous pulse height spectrum, measurements with Sn, Cu and Pb scatterers of different thicknesses were made. The pulse height spectra corrected for different absorption due to different thicknesses and normalized to the same number of atoms are shown in figures 12, 13, and 16. On account of the low counting rate, spectra of pulses greater than 50V were not measured. All the curves show a well resolved peak

due to gammas scattered by the Compton effect but the annihilation peak was not resolved for thin targets. This is easily understandable because the scatterer thickness was smaller than the positron range. This effect is most pronounced in the case of tin (Fig. 13).

(A) Water

The quantity of distilled water used as scatterer was 1780 grams contained in two rectangular milk cartons made of heavy waxed paper. The sides of the scatterer were each approximately 3" x 6" x 6". The side 6" x 6" was placed normally to primary beam of gammas. Thickness of the lead filter used was $1\frac{3}{4}$" and the total number of pile up pulses was negligible.

Because the shape of the scatterer being different from that assumed in deriving eq. (4.4) the correction factor due to absorption is

$$\frac{1}{a} = \frac{1}{XY\tau^2\rho^2}\left(1-e^{-\tau(X\rho)}\right)\left(1-e^{-\tau(Y\rho)}\right) \qquad (5.1)$$

where X = 3" is the thickness of the scatterer and Y = 6" is its width.

(a) Elastic scattering

In Fig. 9 are shown the results obtained. The background counts which are mainly due to scattering from air and the empty carton have been subtracted. The broken line on the figure corresponds to the Co^{60} spectrum normalized and fitted to the experimental points in the already explained

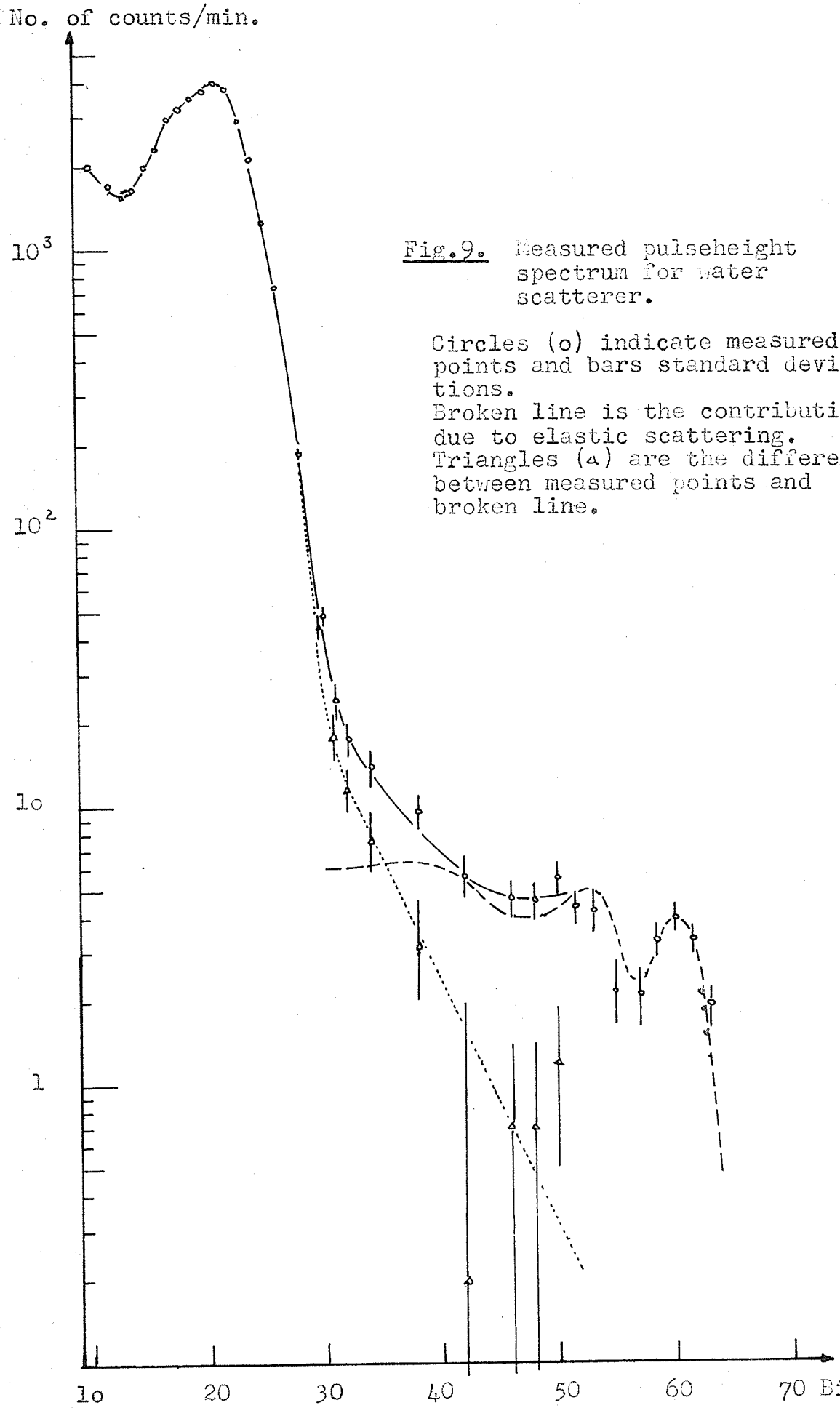

Fig.9. Measured pulseheight spectrum for water scatterer.

Circles (o) indicate measured points and bars standard deviations.
Broken line is the contribution due to elastic scattering.
Triangles (△) are the difference between measured points and broken line.

manner. The broken line shows that this fit is good (within the experimental errors) for the 1.17 MeV peak as well as for 1.33 MeV. The dotted line and the triangular points correspond to the continuous part of the spectrum after the contribution due to elastic scattering was subtracted.

The good fit of the broken line to both peaks (1.33 MeV and 1.17 MeV) shows that the cross section for the elastic scattering is the same within the accuracy of the measurements (about 20%). The correction factor due to absorption of the 1.33 MeV gammas in the scatterer is obtained from eq. (5.1) and has the value $\alpha = 1.94$. The absorption correction for 1.17 MeV line has a slightly greater value ($\alpha = 2.0$) but on account of the low statistical accuracy of the measurements this difference is discarded in the evaluation of cross section.

The cross section obtained for both energies (1.17 MeV and 1.33 MeV) is

$$\frac{d\sigma_{\mu e}}{d\Omega}(90^\circ) = 2.2 \times 10^{-31} \text{ cm}^2/\text{sterad}.$$

The overall possible error in this result is estimated as 35%.

(b) Inelastic scattering

Cross sections for inelastic scattering are shown in Fig. 17. They have been calculated by using eq. (4.14) and the points indicated by triangles in Fig. 9.

(B) Aluminum

The aluminum scatterer had a weight of 626.3 grams.

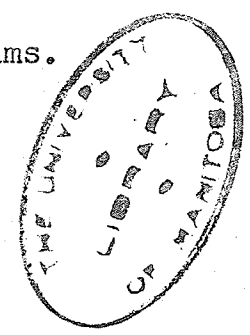

Its size was $5\frac{1}{2}$" x 6" (213.5 cm^2) and its thickness was 2.93 gm/cm^2. The angle φ between the primary beam and the scatterer was 65° . The thickness of the lead filter was 9/8". The material used was aluminum metal of high purity (99.7%). Iron and silicon made up 70% of all impurities.

(a) Elastic scattering

The experimental results are shown in Fig. 10. Background, as measured with the primary beam on and without scatterer, was for all points, especially near the right end of the spectrum, smaller than the standard deviation and it was considered negligible. The number of pulses in the region between 10V and 24V was fairly high so that it produced about 200 pileup pulses per minute with amplitudes between 28V and 45V.

The meaning of the broken line in Fig. 10 is the same as in Fig. 9. It was fitted to the experimental points by assuming that the number of pulses in the tail of the inelastic component, having pulse heights greater than 55V, was negligible in comparison with the number of pulses due to elastic scattering. From the general shape of the curve this assumption does not seem quite justified and so it is likely that the cross section obtained is slightly too high.

Measurements show, within the accuracy of the experiment, that the cross section for elastic scattering is roughly the same for the two Co^{60} lines. The correction due to absorption in scatterer was made according to the eq. (4.4) and for 1.33

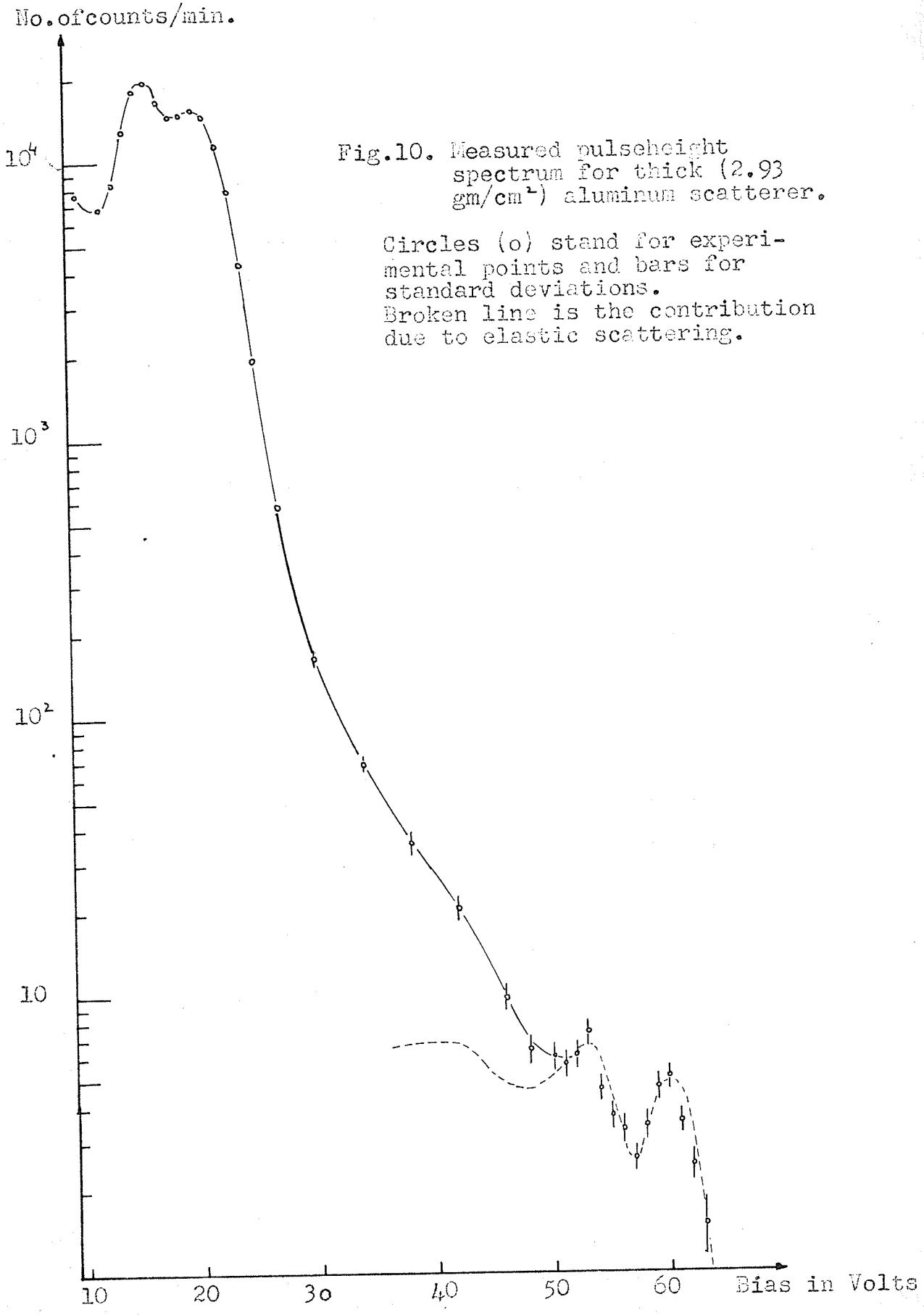

Fig.10. Measured pulseheight spectrum for thick (2.93 gm/cm^2) aluminum scatterer.

Circles (o) stand for experimental points and bars for standard deviations.
Broken line is the contribution due to elastic scattering.

MeV it was $\alpha = 1.29$. By using formula (4.11) and the results from (4.17) (4.18) and table I we get for the cross section for 1.33 MeV (this is also the result for 1.17 MeV because the difference in the absorption correction factor is small as compared to the statistical error) the following value:

$$\frac{d\sigma_{AE}}{d\Omega}(90^\circ) = 6.9 \times 10^{-31} \text{ cm}^2/\text{sterad}.$$

The total error in this result is estimated to be about 30%. It is possible that another systematic error as high as 10% is present due to the tail of inelastically scattered gammas. If so, the true cross section should be smaller than the one indicated above.

(b) Inelastic scattering

The results about the cross section for inelastic scattering that can be inferred from Fig. 10 are very inconclusive owing to high pileup and they are not presented here. All that can be said is they indicate that the cross section for Al is by a factor of two or three greater than for H_2O.

(C) Copper

(a) Elastic scattering

In measuring the elastic component a large scatterer was used. Its total weight was 455.6 gm, area 213.5 cm^2 (6" x 5½") and the corresponding thickness 2.13 gm/cm^2. The lead filter was 9/8" thick. Copper used as material in the scatterer was analytically pure with less than 0.01% of elements with $Z > 29$. The scatterer made an angle of 65° with the primary beam.

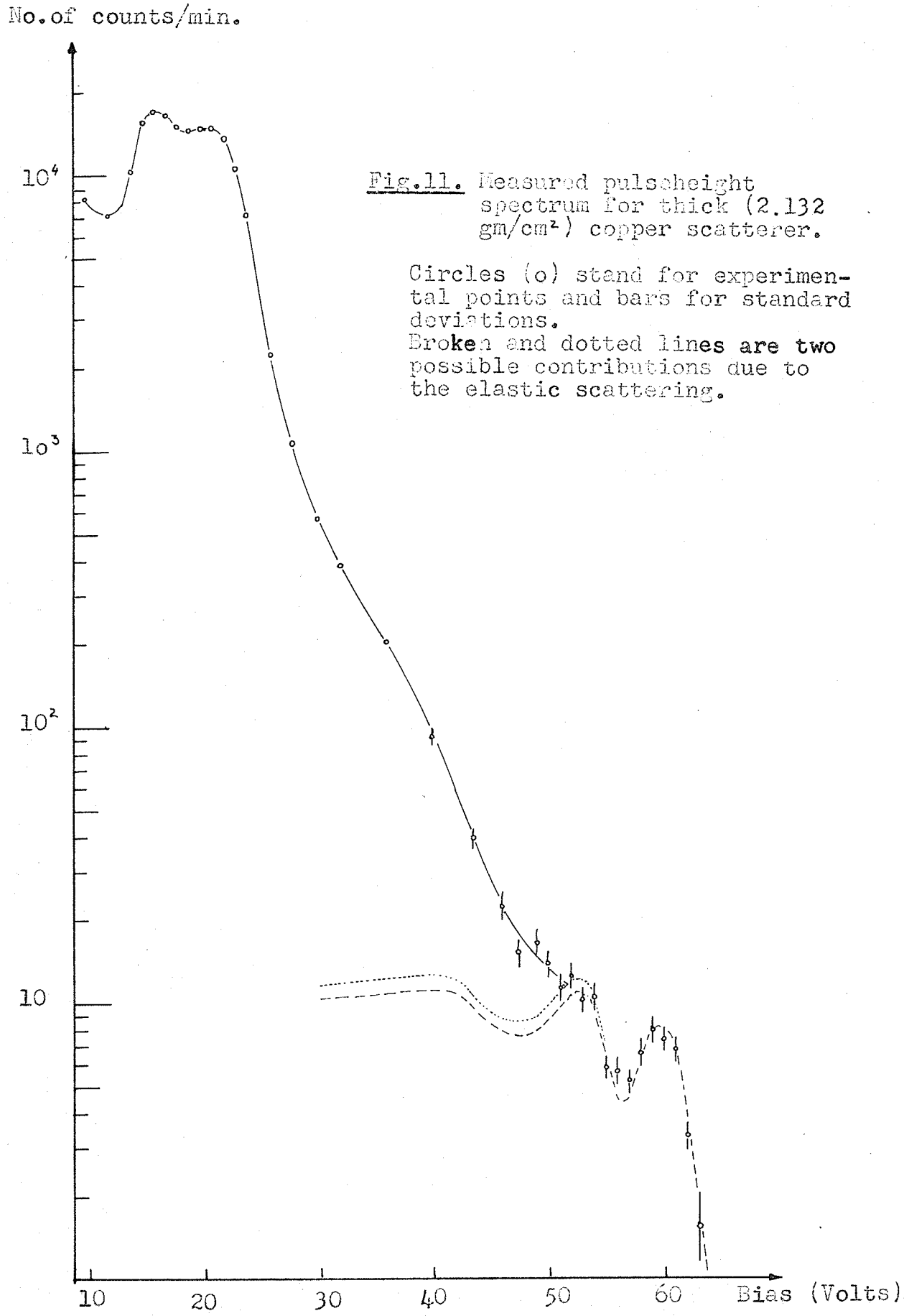

Fig.11. Measured pulseheight spectrum for thick (2.132 gm/cm^2) copper scatterer.

Circles (o) stand for experimental points and bars for standard deviations.
Broken and dotted lines are two possible contributions due to the elastic scattering.

The results of the measurements are shown in Fig. 11. The background was neglected as it was always smaller than 2% of the corresponding counting rate with the scatterer in the beam. The slight increase of about 40V is caused by pile-up of pulses smaller than 26V. However the number of pile-up pulses for pulse heights greater than 48V was again negligible.

The broken line is the elastic scattering. It was fitted to the experimental points as explained before without taking into account the possible presence of a higher energy tail of the inelastically scattered quanta.

As in the case of aluminum we obtain the cross section for 1.33 MeV line

$$\frac{d\sigma_c}{d\Omega}(90,\ 1.33) = (\ 3.5 \pm .9\ ) \times 10^{-30}\ \text{cm}^2/\text{sterad}.$$

Presumably this value is 10%-20% high owing to the presence of inelastic scattering. The accuracy of measurement does not give an unambiguous answer as to the intensity of the 1.17 MeV line since the dotted line fits the experimental results as well as the broken line. For the cross section is taken an average value

$$\frac{d\sigma_c}{d\Omega}(90^\circ,\ 1.17) = (\ 3.7 \pm 1.2\ ) \times 10^{-30}\ \text{cm}^2/\text{sterad}.$$

The indicated errors in both cases are estimated total errors.

(b) Inelastic scattering

Scatterers were made of electrolytic copper foils; purity was unknown but it was believed satisfactory. Three different sizes were used. Area of the scatterer No. 1 was

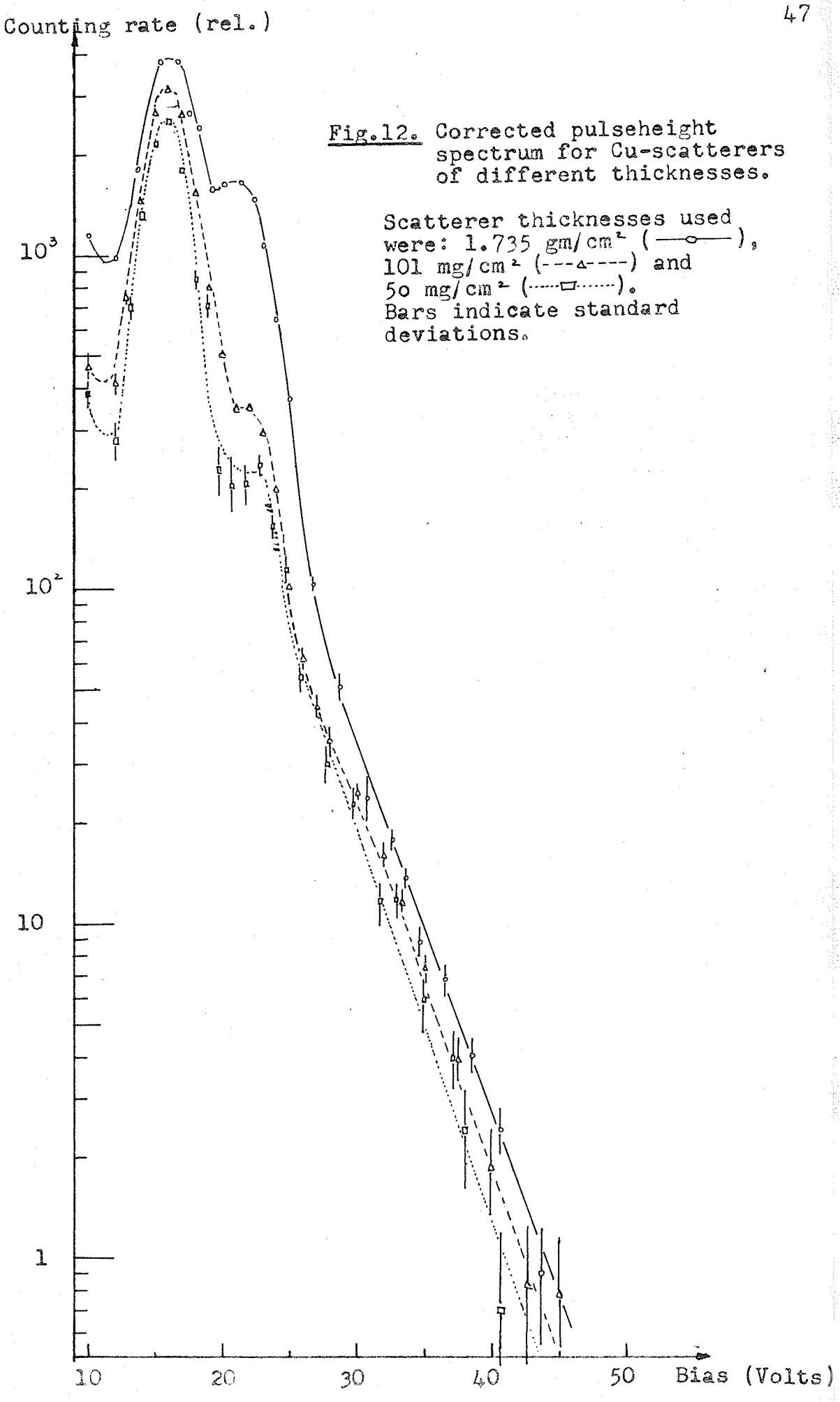

Fig.12. Corrected pulseheight spectrum for Cu-scatterers of different thicknesses.

Scatterer thicknesses used were: 1.735 gm/cm² (—o—), 101 mg/cm² (---△----) and 50 mg/cm² (·····□·····). Bars indicate standard deviations.

213.5 cm^2/or $5\frac{1}{2}$" x 6") and its thickness 50 mg/cm^2 . Scatterer No. 2 had the same area but thickness approximately twice as great (701 mg/cm^2). The third scatterer, No. 3, had a small area 12.35 cm^2 (or $1\frac{1}{2}$" x 1 3/8") but a large thickness, 1.735 gm/cm^2 . The first two scatterers made an angle of 80° with the direction of the primary beam and the third one an angle of only 45° .

Comparative results for all three scatterers are shown in Fig. 12. In the case of scatterer No. 3 the number of counts was corrected for the absorption in it and in the case of No. 1 and No. 2 corrections due to their large sizes were done assuming that $\ell = 0.95$.

Cross sections for inelastic scattering were evaluated for scatterer No. 2 by using eq.(414). Only the energy interval between 550 KeV and 1 MeV was taken into consideration. The results are given in figure 17.

(D) Tin - Inelastic scattering.

Scatterers were made from chemically pure tin metal foils whose percentage of impurities was unknown. Three scatterers of different thicknesses (12 mg/cm^2, 48 mg/cm^2 and 1.53 gm/cm^2) were used. The size of the first two scatterers was 213.5 cm^2 ($5\frac{1}{2}$" x 6") and of the thick one, 6.66 cm^2 .

In Fig. 13 comparative results for all three scatterers are shown under the same conditions as for copper. Exactly the same procedure used in evaluating cross section for copper was applied here, and the results, for scatterer No. 2 (48 mg/cm^2 thick) are presented in Fig. 17.

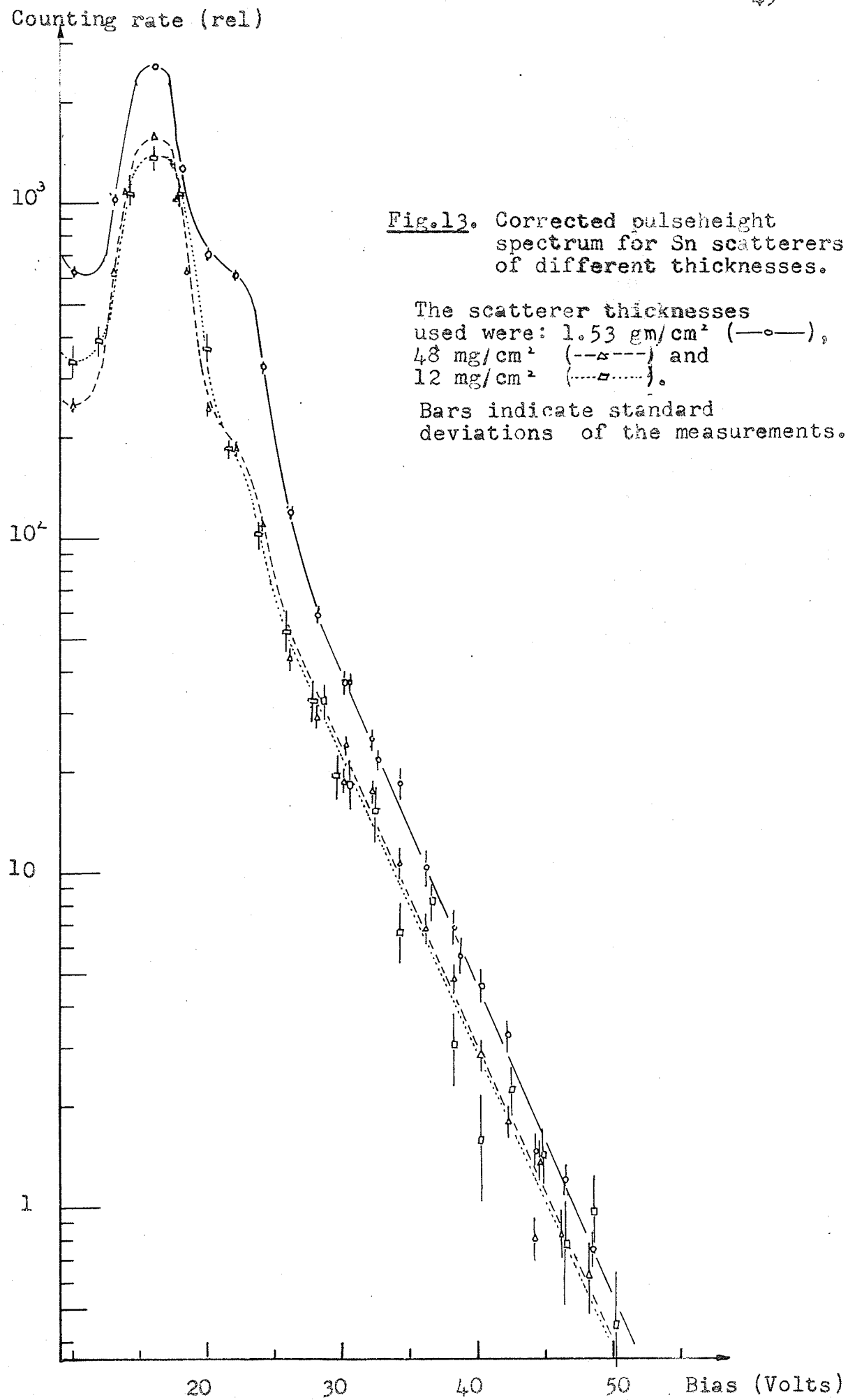

Fig.13. Corrected pulseheight spectrum for Sn scatterers of different thicknesses.

The scatterer thicknesses used were: 1.53 gm/cm² (—○—), 48 mg/cm² (--△---) and 12 mg/cm² (····□·····).

Bars indicate standard deviations of the measurements.

(E) Lead

The experiments on lead were done in order to measure the elastic cross section for both γ-ray line of 1.17 MeV and 1.33 MeV. Also, the inelastic scattering was examined in a much wider energy range than before. The material used was the analytically pure lead metal (in the form of foils) whose total impurities were smaller than 0.002%.

(a) Elastic scattering

In measurements of the elastic component a large scatterer was used. Its area was 144 cm^2 (4 3/4" x 4 3/4") and thickness 1.028 gm/cm^2. It made an angle of 65° with the primary beam. The filter used was 1" thick and the number of pileup pulses for biases greater than 45V was negligible. The channel width used was .75V.

The results of the measurements are shown in Fig. 14. In the region of special interest (for biases greater than 26V) the background was always smaller than 1% and was treated as negligible. Measurements on scatterers of smaller sizes showed that the gentle bow in the region between 30V and 45V was caused by a large number of pileup pulses. The dotted line below the experimental points is the rough correction obtained by comparing measurements with small scatterers and this one. The small peak and the bump correspond to energies of 1.33 MeV and 1.17 MeV respectively.

In order to get cross sections for elastic scattering it was necessary to separate counts due to the 1.33 MeV

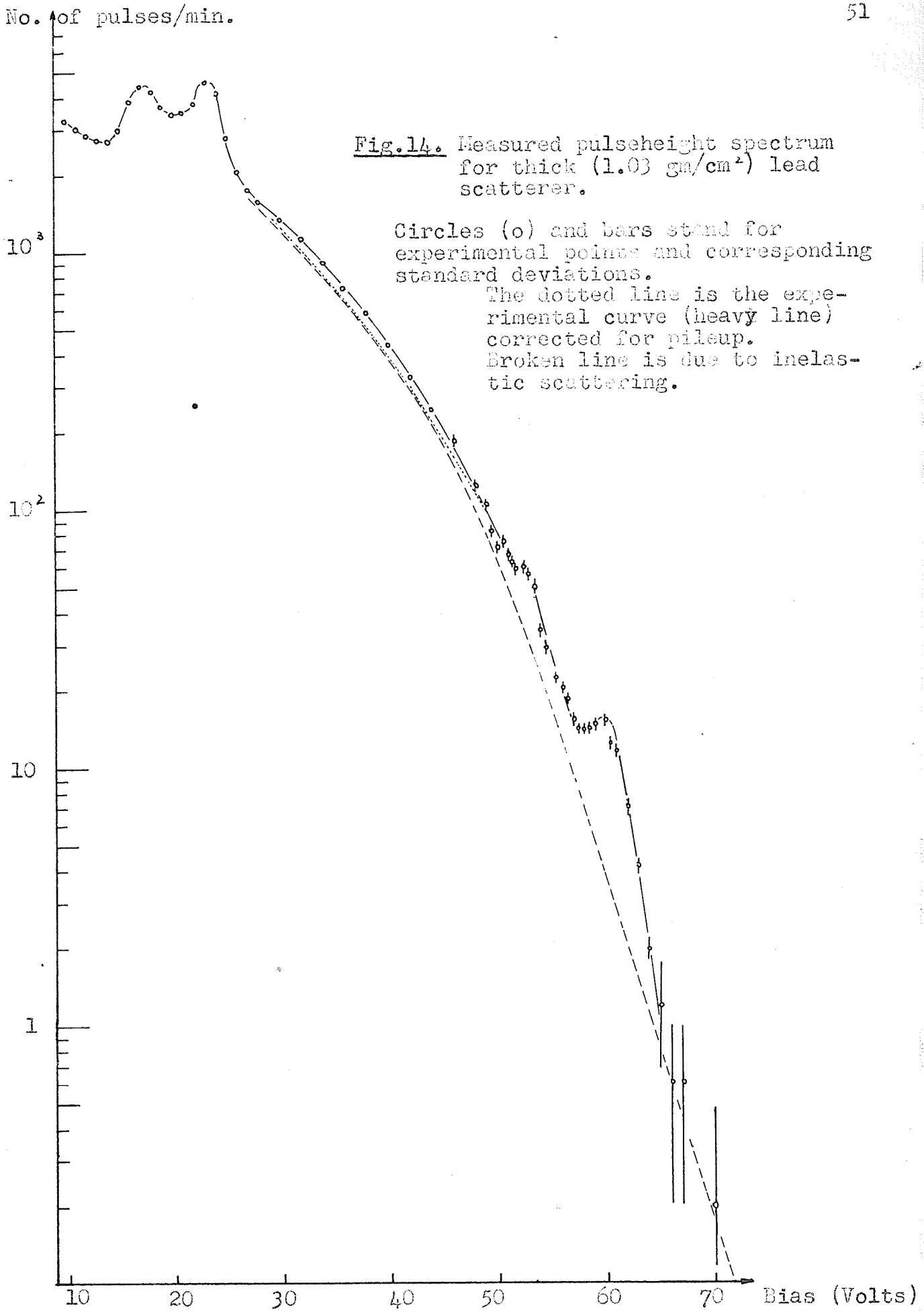

Fig.14. Measured pulseheight spectrum for thick (1.03 gm/cm²) lead scatterer.

Circles (o) and bars stand for experimental points and corresponding standard deviations.
The dotted line is the experimental curve (heavy line) corrected for pileup.
Broken line is due to inelastic scattering.

line and continuous inelastic scattering. The special procedure used is illustrated in Fig. 15 where an enlarged portion of the right side of Fig. 14 is shown. The small circles without bars indicate the measured points. Broken and dotted lines give the approximate pulse height spectrum if only the 1.33 MeV and the 1.17 MeV line, respectively, were present. These spectra were obtained by measuring the spectrum of the small Co^{60} source placed at the centre of scatterer (lead filter used was 1") and analysing it into components with the help of Zn^{65} and Na^{22} spectra obtained under the same conditions. The intensity of these lines, as given in the picture, was so adjusted that the continuous spectra due to inelastic scattering had a smooth shape. This spectrum is indicated in the picture by a heavy line and cross points, and it was obtained by subtracting spectra of 1.33 MeV and 1.17 MeV lines from experimental points. In Fig. 14 the broken line represents the same inelastic spectrum shown in the interval from 26V to 70V.

By this procedure the following results were obtained for N (eq. 4.11):

for 1.33 MeV

$$N_{1.33} = 12 \pm 12\% \text{ counts/min}$$

and for 1.17 MeV

$$N_{1.17} = 25 \pm 25\% \text{ counts/min}$$

By using the following data:

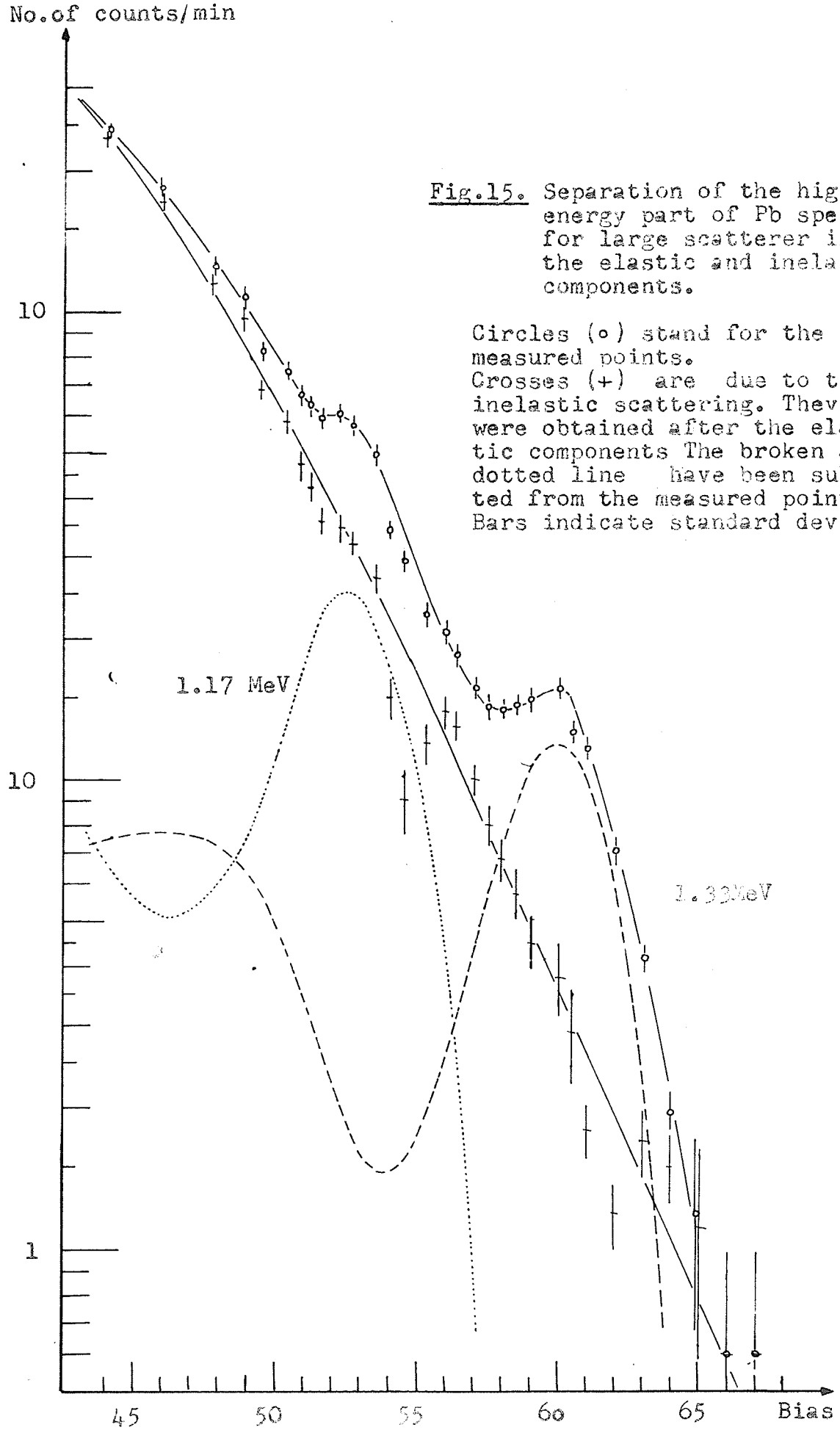

Fig.15. Separation of the high energy part of Pb spectrum for large scatterer into the elastic and inelastic components.

Circles (o) stand for the measured points.
Crosses (+) are due to the inelastic scattering. Thev were obtained after the elastic components The broken and dotted line have been subtracted from the measured points.
Bars indicate standard deviations.

$N_s|_{1.33}$ = 740 c/m $N_s|_{1.17}$ = 880 c/m

$a|_{1.33}$ = 1.10 $a|_{1.17}$ = 1.11

and ϵ = 0.98

r = 92.5 cm

the differential cross sections were obtained

$\frac{d\sigma_{Pb}}{d\Omega}(90°, 1.33 \text{ MeV}) = (1.2 \pm 30\%) \times 10^{-28}$ cm²/ster

$\frac{d\sigma_{Pb}}{d\Omega}(90°, 1.17 \text{ MeV}) = (2.1 \pm 45\%) \times 10^{-28}$ cm²/ster

As before the indicated errors are total estimated errors.

(b) Inelastic scattering

The inelastic scattering was measured by using two different scatterers, one 213.5 cm²(5½" x 6") in area and (68.5 mg/cm² thick, and the other 12.35 cm²(1½" x 1 3/8") in area and 3.16 gm/cm² thick. The pulse height spectra corrected for different absorption in scatterers and normalized to the same number of atoms are presented in Fig. 16. Standard deviations of the points are of the order of the sizes of circles and triangles used. The ordinate is on an arbitrary scale.

The data for thin scatterer were used to obtain the inelastic cross sections in the energy interval between 600 KeV and 1.1 MeV. The corresponding curve (statistical errors are small) is presented in figure 17 (heavy line). The broken line in Fig. 14 was also used to get the cross section in an interval extending so far as from 600 KeV to 1.6 MeV. The result is also represented in Fig. 17 (broken line). The large disagreement between the two lines in the interval between 1.0 MeV and 1.15 MeV can be explained by the fact that

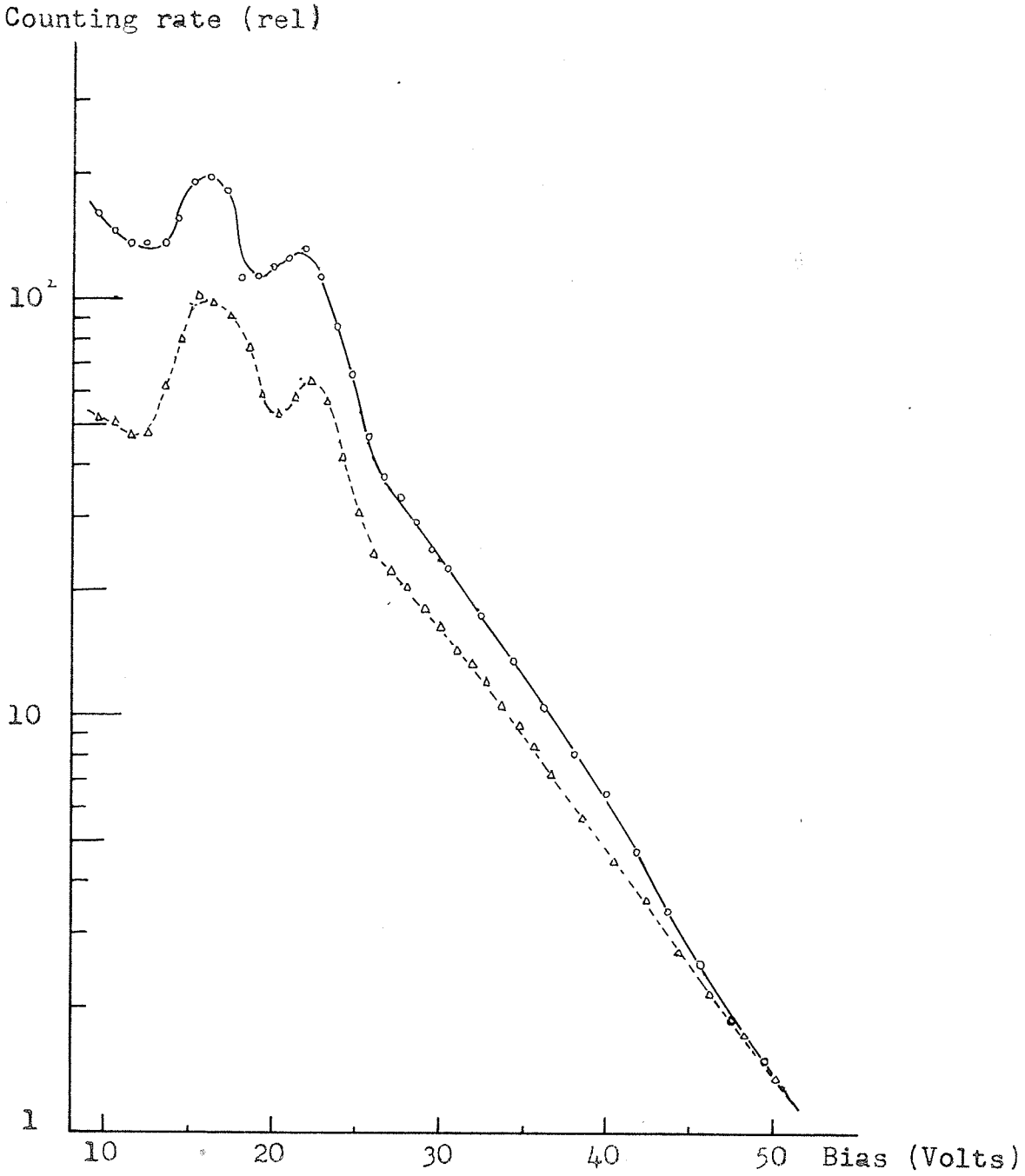

Fig.16. Corrected pulseheight spectrum for Pb scatterers of different thicknesses.

The scatterer thicknesees used were: 3.16 gm/cm² (—o—) and 68.5 mg/cm² (---Δ---). Standard deviations are of the order of magnitude of the circles and triangles used.

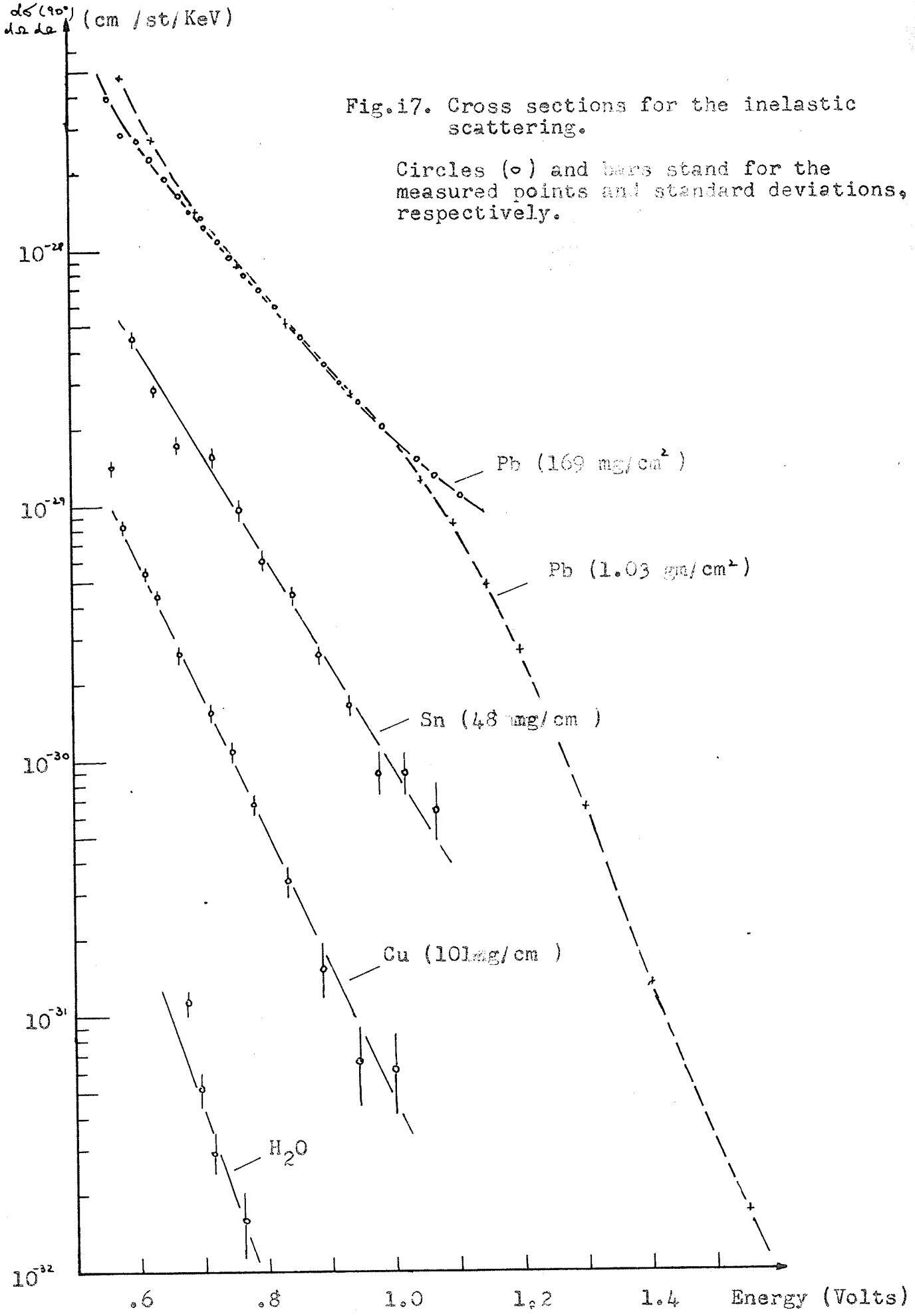

Fig.17. Cross sections for the inelastic scattering.

Circles (o) and bars stand for the measured points and standard deviations, respectively.

counts due to elastic scattering have not been substracted in the case of thin scatterer. The close agreement in the interval between 700 KeV and 1 MeV is probably accidental due to some systematic errors because the scatterers compared were thin and thick and more direct data in Fig. 16 show that some difference should be expected. The shape of the curve far on the right is also questionable due to poor statistics. Neither statistical errors which are small nor systematic errors are shown on the curve but it is estimated that the total error for every point on the curve is smaller than (30%) except far on the right where, owing to poor statistics it amounts to 70% or 100%.

VI. SUMMARY OF RESULTS AND DISCUSSION

(A) Elastic scattering

In Table II we give a comprehensive survey of our results, some measurements published in the literature, and theoretical predictions. In the first five rows the theoretical cross sections are presented: (1) the Thomson cross section $d\sigma_T/d\Omega$ obtained from eq. (2.6); (2) the Franz cross section from eq. (2.11), $d\sigma_F/d\Omega$ (3) the combination of these two as given by eq. (2.12), $d\sigma_{TF}/d\Omega$; (4) the Bethe cross section obtained from the expression for the K-electron scattering amplitude (eq. 2.14) multiplied by 1.2 owing to effects in the L-shell, $d\sigma_B/d\Omega$ and (5) the combined Bethe and Thomson cross section, $d\sigma_{TB}/d\Omega$. In the sixth row results of the present measurements are given and in the seventh row the cross sections published by other authors. All the results listed, if not otherwise stated, refer to the scattering angle of 90° and gamma energies of 1.33 MeV and 1.17 MeV. Indicated errors in the case of our results are the total estimated errors, i.e. due to both statistic and systematic errors.

Comparison of our results with the other results published in the literature shows that in the case of lead there exists good agreement with results from references [15] and [19]. For Cu, Al and H_2O the results cannot be compared because no previous measurements have been done.

Table II shows that there exists better agreement of our results with Bethe's formula than with Franz's especially

TABLE II

Differential Cross Section for the Elastic Scattering of 1.33 MeV and 1.17 MeV photons at 90° in microbarns/steradian

	1.33MeV				1.17 MeV			
Cross section	H_2O	Al	Cu	Pb	H_2O	Al	Cu	Pb
$d\sigma_T/d\Omega$	.215	.430	2.09	12.	.215	.430	2.09	12.7
$d\sigma_F/d\Omega$	.253	1.08	12.1	273	.370	1.58	17.6	400
$d\sigma_{TF}/d\Omega$	.935	2.87	24.7	403.7	1.032	3.66	31.8	555
$d\sigma_B/d\Omega$	2.06×10^{-7}	1.4×10^{-5}	1.44×10^{-2}	173	6.4×10^{-7}	4.15×10^{-5}	345×10^{-2}	347
$d\sigma_{TB}/d\Omega$	.215	.435	2.45	279	.215	.438	2.66	492
Present measurement	.22±.08	.29±.20	3.5±.9	120±35	.22±.08	.69±.25	3.7±1.1	210±90
Other measurements	.15±.04 [17] *	.8±.4 [14]+	4±2 [14]+	120±40 [14]+ 200±60 [11] 800 [13] 135±27 [15] 180±40 [19]				198±40 15=

* This measurement refers to carbon, scattering angle of 130° and to the γ-energy of 1.65 MeV.

\+ This measurement refers to the scattering angle of 135°.

= This measurement refers to the scatering angle of 115°

for low Z . The results for water, where the Rayleigh scattering (according to Bethe's formula) is negligible, is in excellent agreement with the formula for Thomson scattering. The measured cross sections for Cu and Al are higher by about 40% than predicted by eq. (2.16), but the estimated errors are almost as high as the difference, so it could be said that the experimental results are in fairly good agreement with theoretical predictions. In the case of lead the disagreement between experimental and theoretical results is far beyond the estimated errors. It is almost impossible to give the origin of this discrepancy because neither is Bethe's formula exact nor is anything known about the influence of Delbruck scattering that could, due to constructive or destructive interference influence the final results significantly.

(B) Inelastic scattering

From section I it turns out that among all known processes only two can explain inelastic scattering with a continuous energy distribution. These are: bremsstrahlung from photo- and Compton electrons and the Compton effect on bound electrons. Annihilation of positrons in flight, in the case of our geometry, cannot produce such hard gammas as those observed. This is clear from eqs. (2.4) and (2.5) and from the fact that positrons are produced mainly in the forward direction. We shall discuss the two possible explanations

separately and only qualitatively.

(a) Bremsstrahlung

There are several different reasons against the suggestion made in the literature [14, 15, 19, 20] that the continuous medium energy pulse height distribution is produced by bremsstrahlung. These are:

(1) Dependence of the intensity of the inelastic component on the scatterer thickness.

This is the strongest reason and a glance at Figs. (12), (13) and (16) shows that most of the inelastic component remains even for very thin targets (it decreases by 1/3 in the worst case). If its origin is due to bremsstrahlung this difference should be much larger.

It was pointed out in sec. II that photo- and Compton-electrons are strongly peaked in the forward direction and because all thin scatterers made an angle of 80° with the primary beam we may take as a rough approximation that all the electrons traverse the scatterer normally. The thickness of thin scatterers was so small that the electrons produced lose only a small part of their energy in traversing them normally. To illustrate this fact we list in table III the energy loss of 1 MeV electrons in passing normally through the targets used. The data are taken from ref. [9] page 10.

Table III

Energy loss of 1 MeV electrons in traversing scatterers normally

Element		Scatterer thickness in mg/cm²	Energy loss in KeV
Pb		169	170
Sn	No. 1	12	15
	No. 2	48	60
Cu	No. 1	50	65
	No. 2	101	130

If we suppose that electrons are produced uniformly throughout the scatterer (practically true because the absorption of primary radiation in scatterer is negligible) than in the case of Sn -scatterer No. 2. the intensity of bremsstrahlung radiation per atom should be approximately four times as intense as for scatterer No. 1 and in the case of Cu No. 2 twice as intense as for Cu No. 1. From figures 12 and 13 it can be seen that the intensity of the inelastic component stays constant (within the experimental accuracy, i.e. within 30%) in this interval of thicknesses. It is evident that this fact by itself is a strong argument against the assumption that the inelastic component produced is due to bremsstrahlung.

The thickness of the thick targets was always greater than the range of 1.25 MeV electrons (the highest energy electrons). It is fairly hard to say how much more

intense the bremsstrahlung radiation has to be from these targets. From Motz's results [23] it can be seen that the differential cross section for bremsstrahlung is roughly independent of energy in the energy interval between 500 KeV and 1 MeV. Accordingly, it could be estimated that the bremsstrahlung intensity from thick targets should be approximately an order of magnitude more intense than that for the thin targets used (12 mg/cm^2). In the higher energy range (around 1 MeV) this factor should be something smaller. From the figures 12, 13 and 16 it can be seen that such a large difference between thin and thick targets does not exist. The small existing difference indicates that only a minor part of the measured inelastic component can be explained as due to bremsstrahlung.

(2) Measured cross section for bremsstrahlung radiation.

If the assumption is made that all the observed inelastic scattering is due to bremsstrahlung than the data for the cross section in fig. 17 has to be corrected for the fact that the number of electrons producing bremsstrahlung is much smaller than the flux of primary gamma radiation passing through the scatterers. We shall correct only curves for Pb, Sn and Cu targets because their cross sections are obtained from the measurements on thin targets and accordingly these results are the most conclusive. The differential cross section curves (heavy lines) are represented in fig. 18.

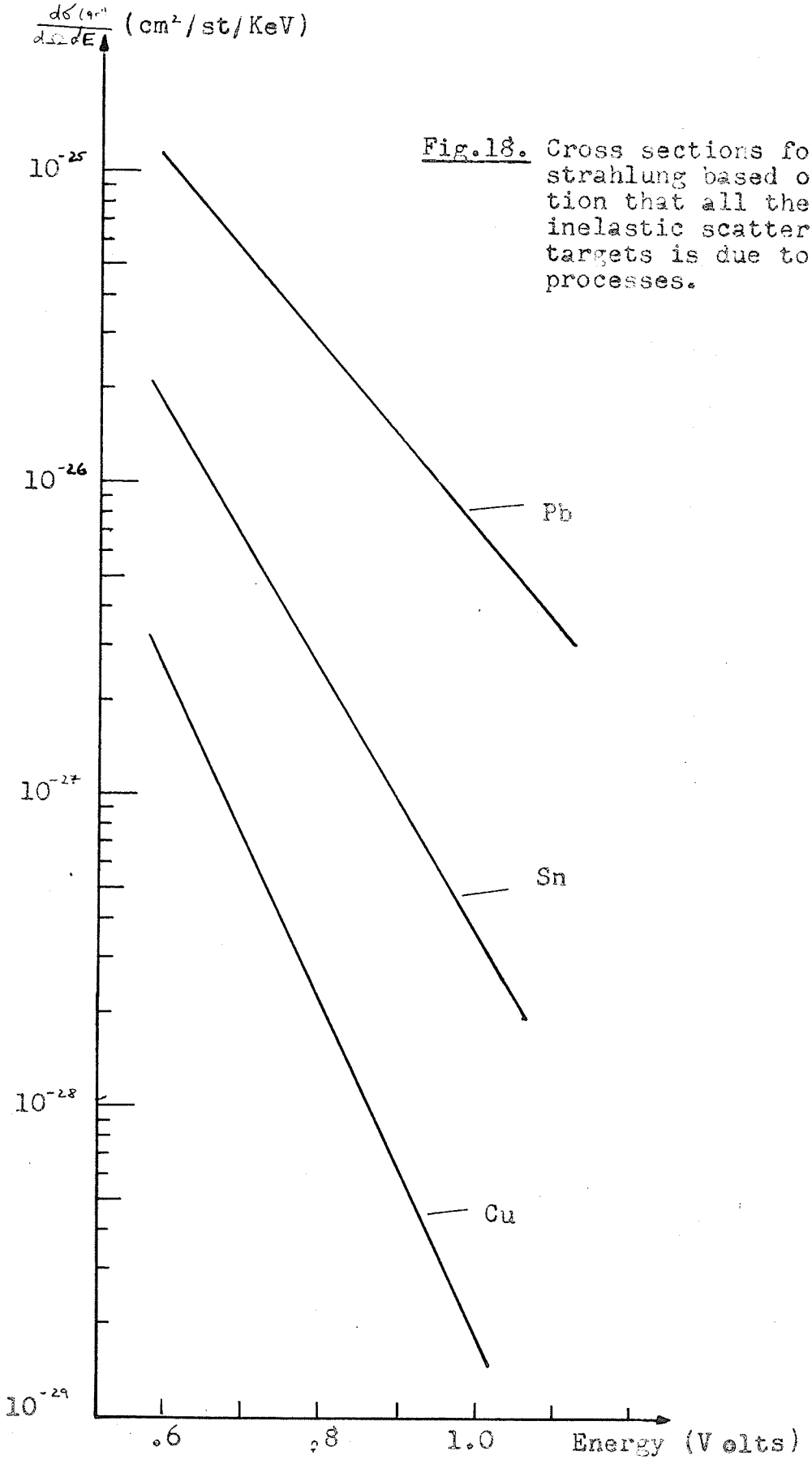

Fig.18. Cross sections for the bremsstrahlung based on the assumption that all the observed inelastic scattering from thin targets is due to secondary processes.

They were obtained from the corresponding curves in fig. 17 by normalizing the thickness of targets used so that the percentage of primary gammas absorbed by photo- and Compton-effect is constant* and then multiplying these curves with the ratio of primary photons passing through the scatterer to the number of electrons produced. By the help of the cross sections for Compton and photo effect (ref. [9] app. I) for Pb, Sn and Cu, it is easy to see that the percentage of radiation absorbed by these two effects for the targets used in Fig. 17 is approximately 1%, .25% and .5%, respectively. If we normalize the thickness of all targets so that .5% of primary radiation is converted into electrons (this is approximately the average value for the targets in consideration) and because they are uniformally produced in the scatterers (the effective thickness of scatterers as seen by electrons is a factor of two smaller) the cross section for assumed bremsstrahlung is obtained by multiplying the curves in Fig. 17 by 400.

Such a simple procedure is a very rough approximation but it is believed it is correct to better than 100% in the high energy region (about 1 MeV). In the lower energy region (around 700 KeV) the real cross section should be smaller than the curves indicate due to the finite angular distribution of photo- and Compton-electrons as well as due to

---

* We may do that because the experiment has shown that the intensity of inelastic component is independent (or only slightly dependent) on the scatterer thickness.

production of Compton electrons with energies lower than 1 MeV. It is hard to estimate this error but likely it is not higher than a factor of two or three.

Comparison of curves in fig. 1 and in fig. 18 qualitatively shows that the cross sections (around 1 Mev) as obtained from our measurements are between one and two orders of magnitude higher than in Motz's experiment. The cross sections for lower energies are again about two orders of magnitude higher. This great discrepancy is another reason against the bremsstrahlung assumption.

(3) Z-dependence of the cross sections in the region of 1 MeV.

The third reason against the bremsstrahlung assumption is the Z-dependence of the cross section in the 1 MeV region. It is easy to see from fig. 18 that the cross section varies approximately as Z^4 instead of Z^2 (corrected by smaller Z' factor) as it is expected for bremsstrahlung.

(c) Compton effect on bound electrons

By applying eq. (2.18) to our results for lead we see that in the case of K electrons only the energy width of the modified line ΔE is equal 285 KeV. Accordingly, we expect that the intensity of inelastic component of 500 KeV energy is $1/82 = 0.0122$ times the intensity at the maximum of the Compton peak. Taking into account the different absorption in lead filter used and the efficiency of the crystal measured ratio should be 0.11 (instead of 0.0122). It is hard to com-

pare this result with measurements in Fig. 16, on account of the presence of the annihilation peak but by interpolating we find that the ratio of intensities is approximately equal to 0.3. The disagreement is fairly large but the higher value should be obtained from the experiment on account of the finite resolution of the spectrometer and fairly large solid angle subtended by scatterer at crystal as well as due to the contribution to the scattering of the electrons in other shells.

In order to obtain a better estimate of the Compton effect on bound electrons we apply eq. (2.20). In Fig. 19 broken lines correspond to the Compton profile of K-electrons only and calculated from this equation. All the curves were so normalized that the contribution at the middle of the Compton peak due to K-electrons was 1/42, 1/25 and 1/13.5 of the contribution due to all electrons for Pb, Sn and Cu respectively. Heavy lines are measured inelastic cross sections reproduced from Fig. 17. We see that qualitative agreement within an order of magnitude exists between the heavy and broken lines. The disagreement becomes serious for energies greater than 900 KeV but here the electrons are highly relativistic - the K-electrons cannot be described by non-relativistic wave functions any longer . Also the nucleus has a finite size which certainly will have the effect of lowering the cross section. The discrepancy at the lower energy (700 KeV) may be understood easily as due to the contribution of L-electrons (and electrons in the other shells) that is not taken into account in eq. (2.20).

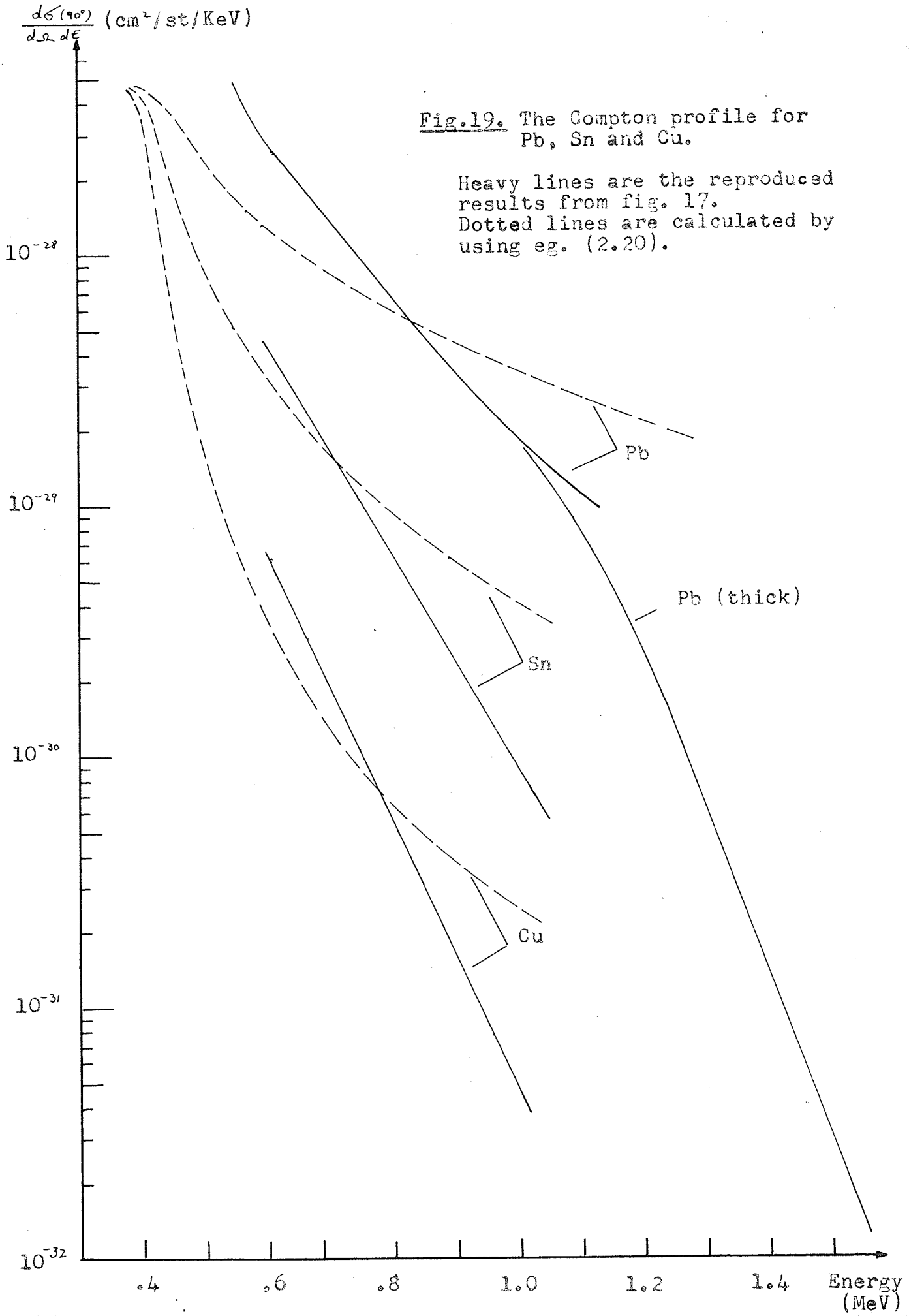

Fig.19. The Compton profile for Pb, Sn and Cu.

Heavy lines are the reproduced results from fig. 17.
Dotted lines are calculated by using eg. (2.20).

From this fairly qualitative discussion it may be concluded that the assumption that the origin of the continuous inelastic distribution of scattered gammas is due to the Compton effect on bound electrons, seems consistent with the results obtained and existing theory.

ACKNOWLEDGEMENTS

The author wishes to express his indebtedness to Professor K.G. Standing for continued guidance, encouragement and help throughout the course of this work. He is also grateful to the Manitoba Cancer Relief and Research Institute, in particular to Dr. R.J. Walton and Mr. T. Griffith for their kind hospitality in the Winnipeg General Hospital and permission to use the Co^{60} -Beam Therapy Unit.

The author is indebted to the National Research Council of Canada for research assistantship which enabled him to study physics at the University of Manitoba. He is grateful to Professors B.G. Whitmore and R.W. Pringle who helped him to get this grant and also to Professor D.K. Jovanovic and to the Council of the Faculty of Science and Mathematics of the Belgrade University for the leave and help that enabled him to come to Canada.

The author also thanks to Professor D. G. Douglas and Professor W. Turchinetz for their kind loan of some equipment used in the experiment.

References

1. W. Heitler, "The Quantum Theory of Radiation", Oxford, 3rd Edition, 1954.

2. A.H. Compton and S.K. Allison, "X-Rays in Theory and Experiment", D. Van Nostrand, 2nd Edition.

3. R. Hofstadter and J.A. McIntyre, Phys. Rev., 16, 1269 (1949).

4. J.W.M. DuMond, Rev. Mod. Phys., 5, 1 (1933).

5. W. Franz, Z. Physik., 98, 314 (1936).

6. J.S. Levinger, Phys. Rev. 87, 656 (1952).

7. E. Segre, "Experimental Nuclear Physics", Wiley (1953), Vol. I, p. 347-348.

8. J.M. Jauch and F. Rohrlich, "The Theory of Photons and Electrons", Addison-Wesley (1955) p. 379-387.

9. K. Siegbahn, "Beta and Gamma Ray Spectroskopy", Interscience Publishers Inc. (1955) p. 521.

10. F.R. Metzger, Phys. Rev., 101, 286 (1956).

11. A. Storuste, Proc. Phys. Soc., 63, 1197 (1950), also Thesis, University of Oslo (1951).

12. R.R. Wilson, Phys. Rev., 82, 295 (1951).
R.R. Wilson, Phys. Rev., 90, 720 (1953).

13. W.G. Davey, Proc. Phys. Soc., A 66, 1059 (1953).

14. T.D. Strickler, Phys. Rev., 92, 923 (1953), also Thesis, Yale University (1952).

15. L. Goldzahl and P. Eberhard, Comp rend., 240, 965, 2304, (1955).

16. J.R. Cook, Proc., Phys. Soc., A 68, 1170 (1955).

17. L.W. Alvarez et al., Phys. Rev., 98, 280 (1955).

18. J.L. Burkhardt, Phys. Rev., 100, 192 (1955).

19. A.K. Mann, Phys. Rev., 101, 4 (1956).

20. S. Messelt and A. Storuste, Proc. Phys. Soc., A 69, 38 (1956).

21. F. Sauter, Ann. d. Phys., 11, 454 (1931).

22. N.B.S. Circular 542--"Graphs of the Compton Energy-Angle Relationship and the Klein-Nishina Formula".

23. J.W. Motz, Phys. Rev., 100, 1560 (1955).

24. H.W. Kendall and M. Deutsch, Phys. Rev., 101, 20 (1956).

25. J.B. Gerhart et al., Phys. Rev., 94, 917 (1954).

26. H.A. Bethe, private communication in ref. [6].

27. F. Rohrlich and N. Rosenzweig, private communication in ref. [6].

28. G.E. Brown and D.F. Mayers, Proc. Roy. Soc., A 234, 387 (1956), and earlier papers.

29. F. Rohrlich and R.L. Gluckstern, Phys. Rev., 86, 1 (1952).

30. J. Toll, Thesis, Princeton University (1952).

31. H.A. Bethe and F. Rohrlich, Phys. Rev., 86, 10 (1952).

32. J.S. Levinger, Phys. Rev., 84, 523 (1951).

33. W.E. Duncanson and C.A. Coulson, Proc. Phys. Soc., A 57, 190 (1945).
C.A. Coulson and N.H. March, Proc. Phys. Soc., A 63, 367 (1950).

34. "Nuclear Level Schemes", U.S. Atomic Energy Commission, T.I.D.-5300.
J.L. Wolfson, Can. J. Phys., 33, 886 (1955).